Journal of Cleaner Production 206 (2019) 180–196

Contents lists available at ScienceDirect

Journal of Cleaner Production

journal homepage: www.elsevier.com/locate/jclepro

# Tuning nanofluids for improved lubrication performance in turning biomedical grade titanium alloy

Saadman Sakib Rahman [a, b, *], Md Zurais Ibne Ashraf [a, b], AKM Nurul Amin [a], M.S. Bashar [b], Md Fardian Kabir Ashik [a], M. Kamruzzaman [c]

[a] Department of Mechanical and Production Engineering, Ahsanullah University of Science and Technology, Dhaka, Bangladesh
[b] Institute of Fuel Research and Development, Bangladesh Council of Scientific and Industrial Research, Dhaka, Bangladesh
[c] Department of Mechanical Engineering, Dhaka University of Engineering and Technology, Gazipur, Bangladesh

ARTICLE INFO

*Article history:*
Received 27 January 2018
Received in revised form
28 August 2018
Accepted 17 September 2018
Available online 18 September 2018

*Keywords:*
Nanofluid
$Al_2O_3$, $MoS_2$, and $TiO_2$ nanoparticles
Ti–6Al–4V ELI
MQCL turning

ABSTRACT

In this paper, two nanofluids suitable for minimum quantity cooling and lubrication (MQCL) assisted turning of Ti–6Al–4V ELI are reported after a comprehensive study of 18 nanofluids. The nanofluids were prepared by adding three different nanoparticles ($Al_2O_3$, $MoS_2$, and rutile-$TiO_2$) to vegetable oils (canola and extra virgin olive oils) respectively, at three different concentrations (0.5, 2, and 4% vol). The use of canola nanofluid containing 0.5 vol% $Al_2O_3$ provided a superior surface finish; on the other hand, canola nanofluid enriched with 0.5 vol % $MoS_2$ was found to be conducive to lowering $T$ and increasing $r_c$. Moreover, the nanofluids rendered an auspicious tool wear behavior and impeded attrition wear. Traces of tribofilm formation and the effect of nano-polishing were identified after examining the finished surface using scanning electron microscopy and energy dispersive x-ray spectroscopy. This analysis also reports on the kinematic and dynamic viscosity, contact angle, contact area and thermal conductivity of the nanofluids, the machined surface morphology, and the improvements concerning surface defects provided by the engineered nanofluids. Finally, the results were compared with those found for dry machining and mineral oil based MQCL turning.



## 1. Introduction

Environmental and occupational health hazards and the effects of rapid global climate change are of growing concerns of the 21st century and apparently these apprehensions have recently led to the establishment of strict government policies and mandates for global manufacturing industries. Researchers working on the metal cutting lubricants have played an active role in cleaning up the environment over the past few decades. Recently, nanofluids, especially vegetable oil (VO) based nanofluids that are suitable for recycling and biodegradation, have been widely explored as potential candidates for replacing mineral and petroleum based cutting lubricants due to their superior tribological performance.

In 2005, nearly 38 million metric tonnes of lubricants were used globally with a projected increase of 1.2% over the next decade (Debnath et al., 2014). European Union alone consumes 320,000 tonnes of metal-working fluids (MWFs) per year and at least two-thirds of which needs to be disposed (Abdalla et al., 2007). It is estimated that MWFs contribute approximately 7–17% of the total machining cost (Klocke and Eisenblätter, 1997). Above all, about 80% of all occupational diseases of operators are due to skin contact with lubricants and, shockingly, estimation shows that in the USA alone about one million workers are exposed to MWFs (Lawal et al., 2012). Thereby, efforts were made by a series of research groups for the development of a replacement of hazardous crude oil based lubricants, and to reduce its' consumption maintaining production efficiency of industries.

Dry cutting is eco-friendly and possesses no risks towards operator health; nevertheless, it falls short to keep up with growing productivity and to maintain quality of the end product especially, in the case of difficult-to-cut materials (Dhar et al., 2006). In consequence, the minimum quantity cooling and lubrication (MQCL) technology has been adopted by worldwide manufacturing industries. The measure is indented to foreshorten profuse flow of the metal cutting lubricant and achieve cleaner production. Furthermore, in contrast to conventional flood cooling and

* Corresponding author. Department of Mechanical and Production Engineering, Ahsanullah University of Science and Technology, Dhaka, Bangladesh.
*E-mail addresses:* saadmans@ualberta.ca, sakibsaad.x@gmail.com (S.S. Rahman).

https://doi.org/10.1016/j.jclepro.2018.09.150
0959-6526/

lubrication technique, MQCL uses only a few milliliters of liquid per hour in the form of tiny droplets (Sidik et al., 2017). Apart from being economical and nature friendly, this technology also provides improved tool wear behavior and better surface finish of the end product after machining (Sharma et al., 2016a).

To further improve lubrication efficacy and relinquish the use of harmful lubricants, vegetable oils (VOs) are being introduced in the last decade (Lawal et al., 2012). There are plenty of scientific articles that seemingly demonstrated the advantages of using VOs in conjunction with MQCL in metal cutting of steels; however, the properties of VOs are in every aspect insufficient to provide effective lubrication during machining of titanium and similar superalloys. Titanium alloys, for example, have low thermal conductivity, high strength and coefficient of friction (COF) at elevated temperature, and poor abrasive and adhesive wear resistance; these thermophysical properties make the cutting process inherently difficult, and are responsible for exceedingly high cutting temperature (Revuru et al., 2017). The heat generated in machining cannot diffuse to its core, as a result, a thin brittle layer (known as white layer) forms in the upper surface layer, which leads to residual stresses. The white layer formation has severe consequences in terms of fatigue life and reliability of the product (Ezugwu and Wang, 1997). Arguably, the droplets of VOs cannot transfer intense heat from the cutting region adequately, thereby, tool condition in such cases exacerbates abruptly. To tackle these issues, nano-size metallic or non-metallic particles can be mixed with VOs. The resulting colloidal solution – known as nanofluid or nanolubricant – renders superior tribological characteristics, and the mechanism through which nanofluids accomplish effective lubrication and cooling is generally expressed by the term 'nanolubrication'.

Nanofluids overcome all these limitations and impart unparalleled improvements of the performance parameters of metal cutting operations. Behera et al. (2016), for example, studied the effect of using $Al_2O_3$ and silver (Ag) nanofluids in MQCL turning of a nickel alloy (Nimonic 90). The researchers reported that the lowest magnitude of cutting force had been recorded while using $Al_2O_3$ nanofluids. Furthermore, they noted that $Al_2O_3$ nanofluid reduced the chip-thickness significantly compared to dry cutting. $MoS_2$ nanofluids were tested by Padmini et al. (2016) in turning of AISI 1040 steel. The authors found that 0.5 vol% of $MoS_2$ enriched coconut oil nanofluid resulted in the reduction of cutting force by 37%, cutting temperature by 21%, tool wear by 44%, and surface roughness by 39%. Vasu and Pradeep Kumar Reddy (2011) compared four cutting conditions (i.e., dry machining, MQCL with pure VO, and MQCL with VO and $Al_2O_3$ nanoparticles) for turning Inconel 600. They inferred that surface roughness, cutting temperature, cutting force, and tool wear can be reduced significantly by using nanofluid assisted MQCL. In another study, Rahmati et al. (2014) compared the performance of $MoS_2$ nanofluid and pure oil in end milling of Al6061-T6 alloy. According to their experimental results, superior surface finish was achieved when 0.5 wt% of $MoS_2$ nanoparticles had been added to pure oil. Sharma et al. (2016b) reported that $TiO_2$ nanofluid, when applied in the form of mist during MQCL turning of AISI 1060 steel, reduced the value of average surface roughness roughly by 47% and 30% compared to dry and conventional MQCL using VO, respectively. Ali et al. (2017) showed that 0.4 wt% of $Al_2O_3$ nanoparticles in soluble cutting oil nanofluid rendered better surface finish in Ti–6Al–4V turning, meanwhile, minimal tool wear was attained for 0.6 wt%. Hegab et al. (2018) studied the performance of multi-walled carbon nanotubes (MWCNTs) enriched vegetable oil based nanofluid in turning of Ti–6Al–4V and reported that 2 wt% of MWCNT nanofluid reduced the power consumption by 11.5% and flank wear of the coated carbide cutting insert by 45% in comparison with tests performed using nanofluids without any carbon nanotubes. The recent progress and applications of nanofluids in MQCL machining processes are distinctively summarized by Sidik et al. (2017) and Debnath et al. (2014).

Perusing the literature reveals that, though Ti–6Al–4V ELI is ubiquitously used for biomedical applications (i.e., implant devices that replace patients' hard tissues) due to high biocompatibility and strength-to-weight ratio, low ion formation levels in aqueous environments, and capability of osseointegration – the mechanical retention of the implant by the host bone tissue – yet there's been surprisingly little research on the enhancement of the machinability of the alloy. Although nanofluids are extensively tested for the metal cutting of steels, a very few scholars have reported on the performance of nanofluids in turning operation of the superalloys, in particular, titanium and nickel alloys. A range of hurdles would have to be considered before commercializing the usage of nanofluids. To illustrate, determination of the accurate concentration of nanoparticles is often extremely complex, since miniscule variation can dramatically alter tribological characteristics of nanofluids. Furthermore, selection of appropriate base fluid is also imperative to overcome perplexity during turning operation of the superalloys. In addition, it is evident that the type of nanoparticles and their thermophysical properties play deterministic roles on the effectiveness of nanolubrication and cooling.

## 2. Methods

### 2.1. Experimental equipment

Turning operation was conducted on a Haas ST-10 CNC lathe (Fig. 1a) using Koves CNMG 120408-AK H01 coated tungsten carbide (WC) cutting inserts (Fig. 1b). A tool-work thermocouple setup for chip-tool interface temperature measurement was developed (Fig. 1c) and a PILOT POWER AB-98 air brush was used as nanofluid spray system (Fig. 2).

### 2.2. Experimental materials

Grade 23, Ti–6Al–4V ELI (extra low interstitials) was chosen as workpiece material. Chemical composition of the alloy is given in Table 1 and a succinct overview of the mechanical, thermal, and electrical properties are stated in Table 2. Alumina ($Al_2O_3$), molybdenum disulfide ($MoS_2$), and rutile-titanium oxide ($TiO_2$) nanoparticles (99.9% purity) were purchased from US Research Nanomaterials, Inc. and used as received. As a bulk material, $TiO_2$ exhibit anatase, rutile, and brookite forms. However, rutile form was chosen in this study as it is thermodynamically the most stable phase, highly biocompatible, has the highest hardness (Rahman et al., 2017) and does not allow reactive oxygen species (ROS) generation after dispersion (Jin et al., 2011). The thermophysical properties and scanning electron microscope images of the nanoparticles are shown in Table 3 and Fig. 2, respectively. Commercially available biodegradable vegetable oils (VOs): canola (CAN) and extra virgin olive (EVO) oils were purchased from a local market in order to use as base fluids. The physical properties and constituents of the VOs are given in Tables 4 and 5, respectively.

### 2.3. Formulation of nanofluids

The nanofluids were prepared (via two-step method) by dispersing the nanoparticles in VOs at three volumetric concentrations (0.5, 2, and 4 vol%). Initially, sonication was conducted for 3 h at room temperature using an ultrasonic bath (Grant XUB 25, 35 kHz and 400 W) to homogenously suspend the nanopartides in the mixtures. Later, to prevent agglomeration or coagulation of the nanoparticles the dispersions were subjected to shear and

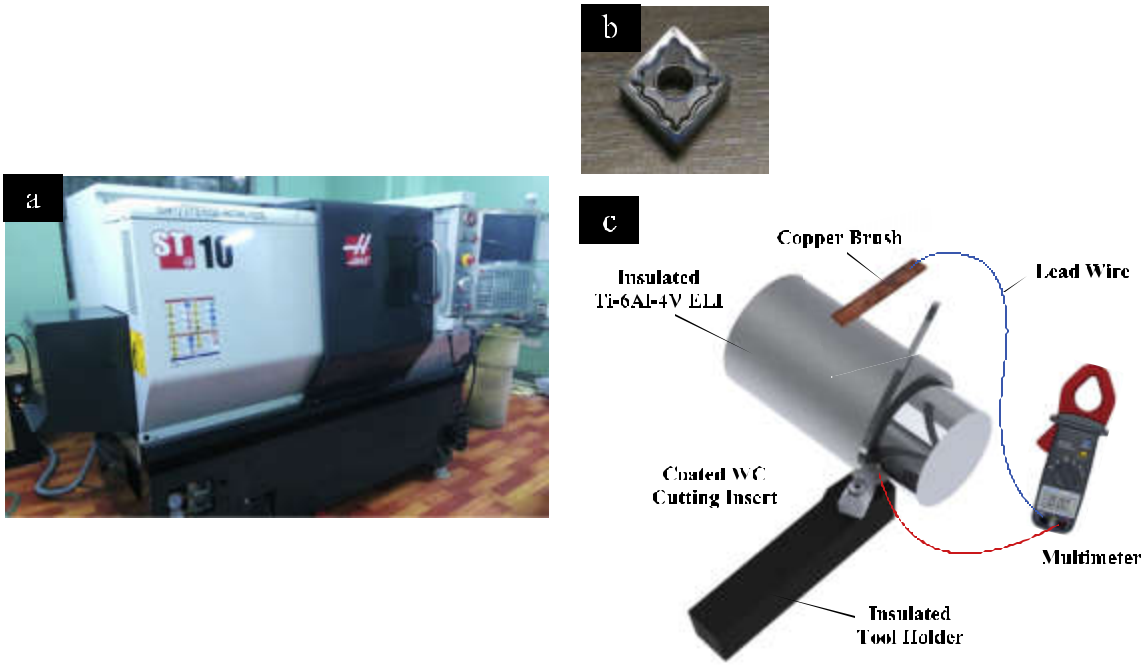


**Fig. 1.** (a) Haas ST10 CNC turning machine, (b) CNMG 120408-AK H01 coated WC cutting insert, and (c) tool-work thermocouple setup for chip-tool interface temperature measurement.

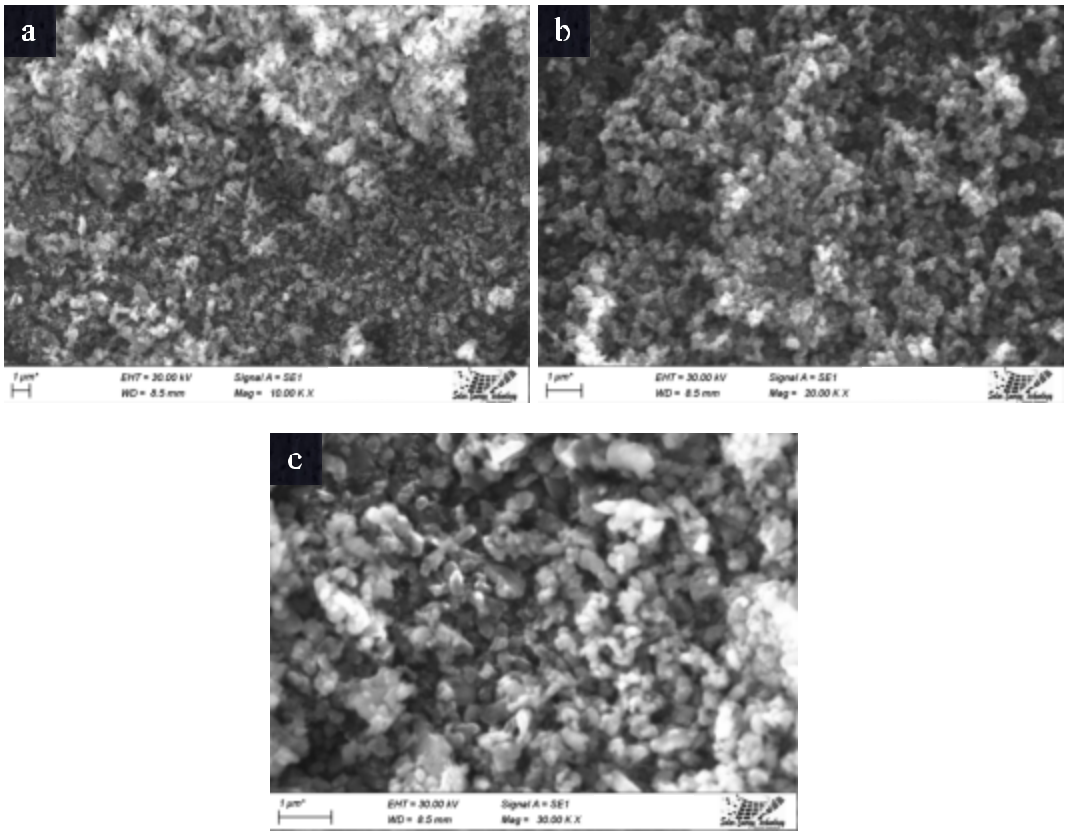


**Fig. 2.** SEM micrographs of (a) $Al_2O_3$, (b) $MoS_2$, and (c) $TiO_2$ nanoparticles.

**Table 1**
Chemical composition (wt.%) of Ti–6Al–4V ELI.

| Element | C | N | Fe | V | Al | Ti | O | H |
|---|---|---|---|---|---|---|---|---|
| wt.% | 0.017 | 0.005 | 0.165 | 3.93 | 5.89 | Balance | 0.128 | 0.00198 |

**Table 2**
Mechanical, thermal, and electrical properties of Ti–6Al–4V ELI.

| | |
|---|---|
| Hardness, Rockwell C | 35 |
| Density | 4.43 g/cc |
| Yield strength | 952 MPa |
| Ultimate tensile strength | 1062 MPa |
| Modulus of elasticity | 114 GPa |
| Thermal conductivity | 6.7 $Wm^{-1}K^{-1}$ |
| Electrical resistivity | 178 μΩ-cm |
| Melting point | 1660 °C |

**Table 3**
The thermophysical properties of the nanoparticles.

| | Size (nm) | $\rho_p$ ($kgm^{-3}$) | $C_p$ ($Jkg^{-1}K^{-1}$) | $k_p$ ($Wm^{-1}K^{-1}$) | $\beta$ ($K^{-1}$) | $\sigma$ $(\Omega m)^{-1}$ |
|---|---|---|---|---|---|---|
| $Al_2O_3$ | 135 | 3970 | 765 | 40 | $0.85 \times 10^{-5}$ | $10^{-10}$ |
| $MoS_2$ | 135 | 4800 | 250 | 138 | $10.7 \times 10^{-5}$ | $10^{-6}$ |
| $TiO_2$ (rutile) | 100 | 4250 | 686.2 | 8.9538 | $0.9 \times 10^{-5}$ | $10^{-12}$ |

turbulent mixing for 30 min using electromagnetic stirrer.

### 2.4. Theoretical calculations using single-phase model

Thermophysical properties of nanofluid can be predicted using two models: single-phase and two-phase model. In the single-phase model, nanofluid is treated as homogenous (single-phase) fluid with steady properties although a mixture of nanoparticles and base fluid is a multi-phase problem. Furthermore, nanofluid is considered to be in thermal equilibrium, and slip velocities between nanoparticles and fluid molecules are omitted. In contrast, properties of nanoparticle and base fluid are considered separately in the two-phase model. It is assumed that nanoparticles and base fluid molecules have distinct velocity and temperature field owing to several factors, such as, gravity, friction between fluid and solid particles, Brownian forces, Brownian diffusion, sedimentation, and dispersion. Hence, the two-phase approach can certainly yield better prediction of the properties of a nanofluid. Nevertheless, many researchers performed numerical simulation using the single-phase approach, and reported acceptable results for heat transfer and other thermophysical properties. For simplicity and ease of computation, numerical simulation of some important thermophysical properties of the nanofluids – likely to influence tribological behavior – were performed following the single-phase approach.

According to Pak and Cho (1998), the density of nanofluid ($\rho_{nf}$) can be determined using equation (1), where $\rho_f$ and $\rho_p$ refer to the densities ($kgm^{-3}$) of base fluid and nanoparticle respectively, and $\varphi$ is the volume fraction of nanoparticle.

$$\rho_{nf} = \rho_f(1-\phi) + \rho_p\phi \quad (1)$$

The specific heat capacity of nanofluid, $(C_p)_{nf}$, was estimated using equation (2) (Pak and Cho, 1998), where $C_f$ and $C_p$ correspond to the specific heat capacities ($Jkg^{-1}K^{-1}$) of base fluid and nanoparticle, respectively.

$$(C_p)_{nf} = (C_p)_f(1-\phi) + (C_p)_p\phi \quad (2)$$

To interpret cooling and heat extraction effectiveness of the nanofluids, thermal conductivity analysis was conducted based on highly cited Bruggeman model (Kim et al., 2004), equation (3). $k_{nf}$ represents the thermal conductivity ($Wm^{-1}K^{-1}$) of nanofluid, and $k_p$ and $k_f$ represent the thermal conductivity of nanoparticle and base fluid, respectively.

$$k_{nf} = 0.25\left[(3\phi-1)k_p + \{3(1-\phi)-1\}k_f + k_f\sqrt{\Delta_B}\right] \quad (3)$$

$$\Delta_B = \left[\frac{(3\phi-1)k_p}{k_f} + \{3(1-\phi)-1\}\right]^2 + \frac{8k_p}{k_f}$$

The Bruggeman equation has been chosen as it is proven to produce accurate prediction of the thermal conductivity of the nanofluids. For instance, Padmini et al. (2016) experimentally measured thermal conductivity of 0.5 vol% CAN-$MoS_2$ nanofluid to be 1819 $Wm^{-1}K^{-1}$. The predicted value of the thermal conductivity of the nanofluid using equation (3) is very close to the experimental value, which is about 1829 $Wm^{-1}K^{-1}$.

**Table 4**
Physical properties of CAN and EVO oils.

| Parameter | CAN | EVO |
|---|---|---|
| Density ($kgm^{-3}$; 20 °C) | 920.2 | 917.2 |
| Heat capacity ($Jkg^{-1}K^{-1}$; 20 °C) | 1837 | 2000 |
| Thermal conductivity ($Wm^{-1}K^{-1}$; 20 °C) | 0.166 | 0.17 |
| Dynamic viscosity (mPa.s; 40 °C) | 25.3 | 25.6 |
| Kinematic viscosity ($mm^2/s$; 20 °C) | 78.2 | 78.5 |
| Smoke point (°C) | 220–230 | 210 |
| Flash point, open cup (°C) | 275–290 | 315 |

**Table 5**
Constituents of CAN and EVO oils.

| Compound | CAN | EVO |
|---|---|---|
| Oleic acid | 62% | 71% |
| Linoleic acid | 21% | 3.5–21% |
| Alpha-linolenic acid | 9–11% | < 1.5 |
| Saturated fatty acids | 7.4% | – |
| Palmitic acid | 4% | 7.5–20% |
| Stearic acid | 2% | 0.5–5% |

### 2.5. Experimental scheme

Air-atomized nanofluid was jetted to the entire rake face and partially to the flank face following the criteria of minimum quantity cooling and lubrication (MQCL). Air-assisted atomization was chosen over ultrasonic atomization, as the latter is less beneficial to the reduction of Leidenfrost temperature effect (Leidenfrost, 1966). Fig. 3 illustrates a section view of the nanofluid spray system. The system is equipped with a gravity feed container and two coaxial nozzles of different diameters. The main nozzle's orifice diameter is 0.3 mm. Air supply pressure and flow rate were set at 6 bar and 120 ml/h respectively in order to achieve better penetration of the nanofluid droplets to contact interfaces and uniform droplet distribution. The nanofluid spray system was positioned approximately 35 mm away from tip of the cutting insert with an impingement angle of 30°.

The $R_a$, $T$, and $r_c$ values were measured at three levels of cutting speed, $v_c$ (55, 80, and 105 m/min). For tool wear observations, $v_c$ of 105 m/min was selected. After 200 mm of turning cutting inserts were analyzed. All the tests were carried out at constant feed rate (0.1 mm/rev) and depth of cut (1 mm). Each experimental runs

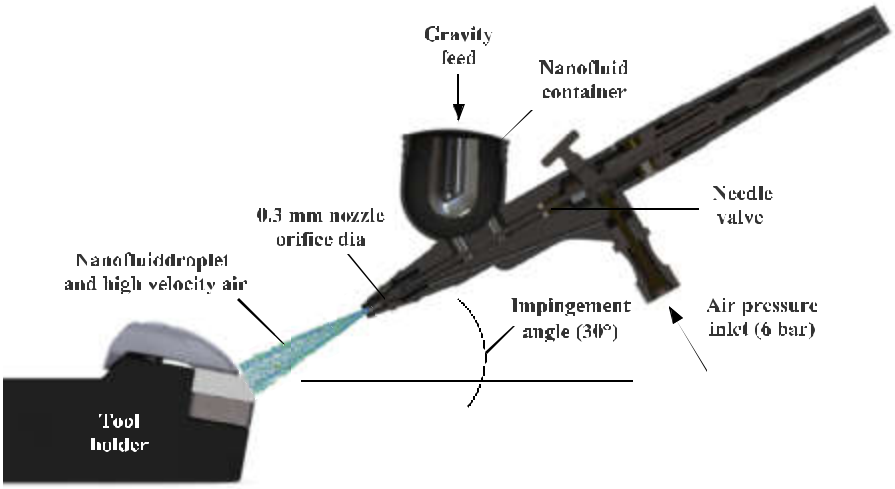


**Fig. 3.** Schematic of the nanofluid spray system in turning setup.

were conducted three times and the average value of the responses were considered for further study.

### 2.6. Characterization equipment

Kinematic viscosity of the nanofluids were measured at 40 and 100 °C temperature using capillary tube viscometer (300). Dynamic viscosity values have been measured using JP SELECTA ST-2020 R. Droplet profiles of the nanofluids and two VOs were captured ~2 s after being dropped on a glass surface (ethanol and water cleaned) following static sessile drop method. Measuring contact angles of sessile droplets directly by the conventional method of placing a tangent to an image of the sessile drop is not free of error. The error arises from the fact that it is difficult to draw the tangent correctly on the image at the liquid–solid–gas interface. Therefore, contact angle was measured by ImageJ 1.51 k using Low Bond Axisymmetric Drop Shape Analysis (LBADSA). The contact angle measurement setup was calibrated against water contact angle (26°) on glass (ethanol and water cleaned) (Shahidzadeh et al., 2015). Scanning electron microscopy (SEM) images and energy dispersive x-ray spectroscopy (EDS) spectrums were collected on EVO 18 Research (Carl Zeiss) equipped with TEAM™ EDS (EDAX) system, using accelerating voltage of 20 kV. Bruker DektakXT stylus profiler with 12.5 μm stylus radius and 3 mg stylus force was used for surface roughness, $R_a$ (the arithmetic average deviation from the mean line within the assessment length of 2 mm) measurements and to generate 3D surface maps. To prevent anomalies, five readings were taken for each turn at five different reference points 60° apart and the average was used for the final evaluation of the surface quality. Chip-tool interface temperature was measured using tool-work thermocouple technique following the procedure described by (Hoyne et al., 2015) and (Kamruzzaman et al., 2017). Carl Zeiss Stemi 508 Stereo microscope was used to acquire the optical images.

## 3. Results

### 3.1. Basic properties of the nanofluids

Density is deemed one of the important parameters, as it influences Reynold's number, Nusselt number, and specific heat of nanofluid. The addition of nanopartides unambiguously raised the overall density of VOs (Tables 6 and 7). Furthermore, increasing the vol%, resulted in an increase of the $\rho_{nf}$. The reduction of the $(C_p)_{nf}$, on the other hand, is apparent with the increase in vol%. The decrease is obvious as nanoparticles have lower specific heats with respect to the base fluids. This behavior was also reported in the previous studies conducted by Chieruzzi et al. (2013) and Zhou and Ni (2008). As can be seen in Tables 3 and 4 that $Al_2O_3$, $MoS_2$, and $TiO_2$ nanoparticles have thermal conductivities of 40, 138, and 8.9538 $Wm^{-1}K^{-1}$, while the thermal conductivities of the VOs are significantly lower, that are, 0.166 and 0.17 $Wm^{-1}K^{-1}$ for CAN and EVO, respectively. The results demonstrate that the addition of nanoparticles is an effective route to enhance the thermal conductivity since the nanofluids manifested moderate improvement over pure VOs. For instance, the maximum thermal conductivity (0.1931 $Wm^{-1}K^{-1}$) was recorded for 4 vol% $MoS_2$-EVO, which is 13.59% higher than the thermal conductivity of pure EVO. In accordance to several studies, an increasing trend in thermal conductivity of the nanofluids with the upsurge in vol% (in the range of 0.5–4 vol%) was observed. Kinematic and dynamic viscosities of the nanofluids are determined through experiments as mathematical models fail to predict the property accurately. Fig. 4 illustrates that the kinematic viscosity (cSt) of the nanofluids enhanced as the vol% is increased. The reason for the increase in kinematic viscosity is the strengthening of the van der Waals attraction between the nanoparticles and viscous interactions between the fluid and nanoparticles possibly due to aggregation of particles at low shear rates. Moreover, spacing between the nanoparticles in nanofluids narrows while vol% enhances, which eventually increases the probability of stochastic collision and increases attraction by Brown random force and colloidal force. Similar trend can also be found in Fig. 5 which shows the comparison of the dynamic viscosity values of the nanofluids. Moreover, nanofluids generally show Newtonian behavior when temperature is higher than 273 K (Sahoo et al., 2009; Yadav et al., 2017).

Contact angle ($\theta$) and contact area of the nanofluid sessile droplets are stated in Table 8. To illustrate the measuring technique a sample of a droplet is shown in Fig. 6. The experimental observations reveal that CAN (79.3°) and EVO (82.77°) have much higher $\theta$ than that measured for almost all of the nanofluids. Viscosity and θ of the nanofluids are inextricably linked. Less viscous nanofluids spread and thinned more hence, smaller contact angles were documented for the nanofluids with lower kinematic/dynamic

**Table 6**
Thermophysical properties calculated for the nanoparticles dispersed in CAN.

| Nanoparticles | $Al_2O_3$ | | | $MoS_2$ | | | $TiO_2$ | | |
|---|---|---|---|---|---|---|---|---|---|
| vol% | 0.5 | 2 | 4 | 0.5 | 2 | 4 | 0.5 | 2 | 4 |
| $\rho_{nf}$ | 935.45 | 981.19 | 1042.19 | 939.6 | 997.79 | 1075.39 | 936.84 | 986.79 | 1053.39 |
| $(Cp)_{nf}$ | 1831.64 | 1815.56 | 1794.12 | 1829.06 | 1805.26 | 1773.52 | 1831.25 | 1813.98 | 1790.96 |
| $k_{nf}$ | 0.1685 | 0.1765 | 0.1882 | 0.1685 | 0.1767 | 0.1885 | 0.1683 | 0.176 | 0.1872 |

**Table 7**
Thermophysical properties calculated for the nanoparticles dispersed in EVO.

| Nanoparticles | $Al_2O_3$ | | | $MoS_2$ | | | $TiO_2$ | | |
|---|---|---|---|---|---|---|---|---|---|
| vol% | 0.5 | 2 | 4 | 0.5 | 2 | 4 | 0.5 | 2 | 4 |
| $\rho_{nf}$ | 932.46 | 978.26 | 1039.31 | 936.61 | 994.86 | 1072.51 | 933.86 | 983.85 | 1050.51 |
| $(Cp)_{nf}$ | 1993.82 | 1975.3 | 1950.6 | 1991.25 | 1965 | 1930 | 1993.43 | 1973.72 | 1947.45 |
| $k_{nf}$ | 0.1726 | 0.1807 | 0.1928 | 0.1726 | 0.1808 | 0.1931 | 0.1724 | 0.1802 | 0.1916 |

viscosity.

### 3.2. Surface roughness

Surface roughness ($R_a$) measurements reveal a noticeable change with the types of nanofluids; $v_c$, on the other hand, played a moderate role. As illustrated in Fig. 7, $R_a$ gradually decreased with the augmentation of $v_c$, while increase in vol% led to degradation of surface finish. To illustrate, 0.5 vol% of $MoS_2$-CAN nanofluid reduced $R_a$ by 8.1% and 10.26% compared to 2 and 4 vol% respectably, at 55 m/min of $v_c$, while the reduction is 3.34% and 6.7% respectively, at 105 m/min (Fig. 7b). Further, CAN manifested lower $R_a$ than EVO, irrespective of $v_c$ and vol%. At 105 m/min, for example, when 0.5 vol% $TiO_2$ was mixed with CAN, the resulted nanofluid set forth a decrease of 3.31% in $R_a$ collated to that quantified for the EVO based nanofluid (Fig. 7c). In the entire experimental domain, the lowest $R_a$ value (0.248 μm) was recorded for 0.5 vol% $Al_2O_3$-CAN nanofluid (Fig. 6a). Subsequently, $R_a$ values obtained for the nanofluids are compared with dry cutting and M-MQCL (Fig. 7d). Not surprisingly, the nanofluids provided better surface finish; nonetheless, the extent of difference in $R_a$ with dry cutting and M-MQCL is remarkable. For instance, the proportion of reduction at 55 m/min of $v_c$ compared to dry cutting are 73.1%, 60%, and 51.2% for 0.5 vol% $Al_2O_3$-CAN, 0.5 vol% $MoS_2$-CAN, and 0.5 vol% $TiO_2$-CAN; however, M-MQCL accounted for only 26.5% reduction. Significant attenuation of $R_a$ was also noted at 105 m/min of $v_c$.

After dry cutting, severe plastic deformation, large area exfoliation, micro-plowing, furrows, adhered microchip debris, and irregular friction tracks were identified on the machined surface of the titanium alloy as shown in Fig. 8a. Additionally, galling – a form of wear caused by friction and adhesion between sliding metallic surfaces – appeared on the finished surface. Galling is distinct from gouging or scratching and more or less similar to cold welding process as material transfers from one surface and permanently or temporarily adheres to the opposite surface. Nanofluids provided highly smooth surface texture, and interestingly, no traces of surface defects were spotted for 0.5 vol% $Al_2O_3$-CAN nanofluid (Fig. 8b). Moreover, absence of scuffing wear – the preferred term when galling wear occurs at lubricated surfaces – is an indication of enhanced galling or scuffing resistance of the titanium alloy. Furthermore, uniform nano-scale friction tracks engraved by very hard $Al_2O_3$ nanoparticles are obvious on the surface, indicating nano-polishing effect (see Discussion). The surface conditions of the workpiece after 0.5 vol% $MoS_2$-CAN and 0.5 vol% $TiO_2$-CAN nanofluid-MQCL assisted turning are shown also in Fig. 8c and d, respectively.

The surface morphology was also investigated by 3D surface profiles (Fig. 9) to state the degree of improvement imparted by 0.5 vol% $Al_2O_3$-CAN nanofluid assisted MQCL over dry cutting mode. In addition to the presence of cold-welded chip-materials, the combination of high cutting zone temperature with high COF inevitably led to ridges and valleys having larger height and non-uniform texture on the surface after dry cutting.

Traces of tribo-film formation on the finished specimens were

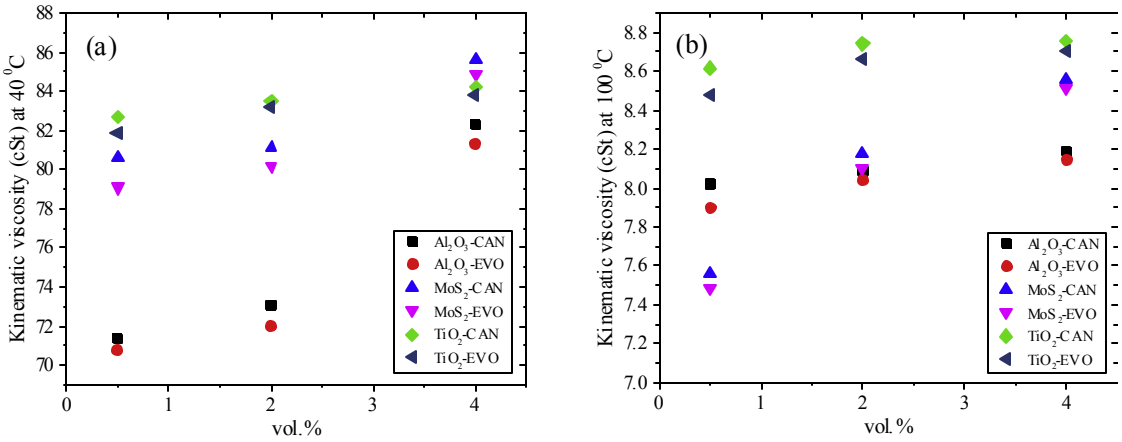


**Fig. 4.** Kinematic viscosity of the nanofluids at (a) 40 °C and (b) 100 °C.

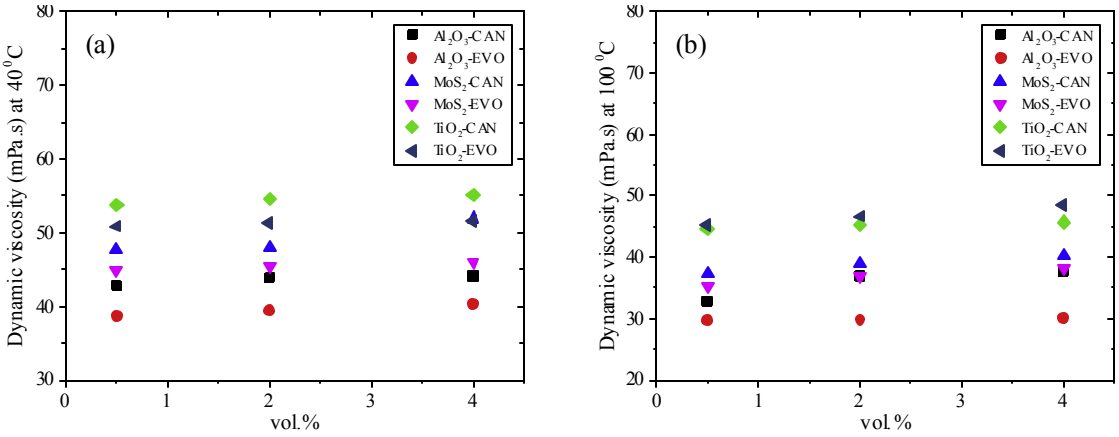


**Fig. 5.** Dynamic viscosity of the nanofluids at (a) 40 °C and (b) 100 °C.

**Table 8**
The contact angle (°) and Contact area ($mm^2$) measurements.

| Nanoparticle | VO | vol% | Contact angle (°) (average deviation ±4%) | Contact area ($mm^2$) |
|---|---|---|---|---|
| $Al_2O_3$ | CAN | 0.5 | 57.63 | 1.85 |
| | | 2 | 67.68 | 1.62 |
| | | 4 | 87.65 | 1.33 |
| | EVO | 0.5 | 55.42 | 1.88 |
| | | 2 | 63.72 | 1.7 |
| | | 4 | 88.27 | 1.27 |
| $MoS_2$ | CAN | 0.5 | 50.75 | 2.07 |
| | | 2 | 61.75 | 1.73 |
| | | 4 | 71.08 | 1.42 |
| | EVO | 0.5 | 50.85 | 2.01 |
| | | 2 | 64.78 | 1.69 |
| | | 4 | 84.53 | 1.39 |
| $TiO_2$ | CAN | 0.5 | 50.86 | 2.07 |
| | | 2 | 61.17 | 1.74 |
| | | 4 | 64.29 | 1.69 |
| | EVO | 0.5 | 55.89 | 1.87 |
| | | 2 | 64.48 | 1.69 |
| | | 4 | 67.44 | 1.62 |

explored through EDS spot analysis (Fig. 10). The detection of tribo-film after turning process is quite difficult as major portion of the lubricating film is scrapped or carried away with deformed chips and the sliding motion of cutting insert. However, traces of the film can be identified through scrutinizing the corresponding EDS spectra. Referring to Table 1, aluminum (Al) and oxygen (O) content (weight percentage) on Ti−6Al−4V ELI are around 5.89 and 0.128%, respectively. The element analysis of the machined surface lubricated with 0.5 vol% $Al_2O_3$-CAN nanofluid reveals a slight increase in Al content, while O content augmented substantially. Thus, it seems likely that traces of tribo-film containing $Al_2O_3$ nanoparticles are present. Likewise, presence of a scant amount of Mo (molybdenum) also supports the hypothesis (see Discussion) about the formation of tribo-film between contact surfaces. Noteworthy, remnant of sulfur (S) couldn't be identified on the investigated portion of the surface through EDS analysis. Although several attempts were made to explore this unusual phenomenon, no conclusive evidence has been obtained in this regard, which warrants further investigation. On the other hand, increase in O content infers oxidation of the tribo-film. According to (Tannous et al., 2011), in the case of $MoS_2$, the oxidation phenomenon could provide oxide like $MoO_3$, which facilitates the adhesion of $MoS_2$ nanoparticles or nanosheets on the sliding surfaces, consequently, strengthens the tribo-film. The O content increased from 0.128% to 17.3% in the surface lubricated by 0.5 vol% $TiO_2$-CAN. Perhaps such upsurge in O content implies the manifestation of tribo-film consists of titanium oxides.

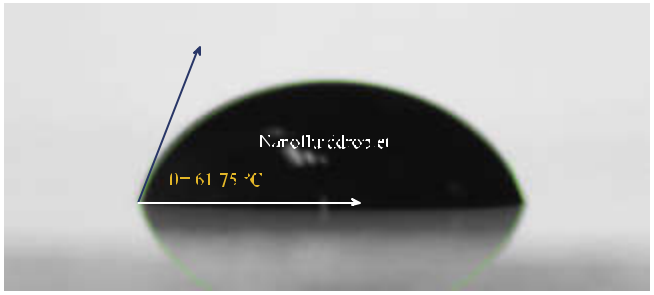


**Fig. 6.** Droplet contact angle measurement of 2 vol% $MoS_2$-CAN nanofluid.

### 3.3. Chip-tool interface temperature

Chip-tool interface temperature ($T$) measurements reaffirms that vol% confers substantial influence on the nanolubrication and cooling performance of the nanofluids; the effect of base fluids, on the other hand, was also conspicuous. It is apparently seen that (Fig. 11), $T$ increases dramatically with vol% (excluding $Al_2O_3$-EVO nanofluids) and, as expected, with $v_c$—mainly owing to the extended chip-tool contact region, which led to higher COF. Overall, when CAN was combined with $Al_2O_3$ (at low cutting speed), $MoS_2$, and $TiO_2$ nanoparticles, the resulting nanofluids provided better heat dissipation. Surprisingly, however, $Al_2O_3$ nanoparticles performed better in conjunction with EVO at medium and high cutting speed. The lowest $T$ was recorded for 0.5 vol% $MoS_2$-CAN nanofluid application, which is ~875 °C. In comparison with dry cutting (at 80 m/min $v_c$), 7.69%, 9.34%, 15.89%, and 8.41% reduction were quantified for M-MQCL, 2 vol% $Al_2O_3$-EVO, 0.5 vol% $MoS_2$-CAN, and 0.5 vol% $TiO_2$-CAN, respectively.

### 3.4. Chip morphology

Chip-thickness values were collected after each run and were used to calculate chip-thickness ratio ($r_c$) using equation (4), which is the ratio of uncut thickness ($t_o$) to deformed chip thickness ($t_c$) (Altintas, 2012).

$$r_c = \frac{t_o}{t_c} = \frac{s_o(\sin\phi)}{t_c} \tag{4}$$

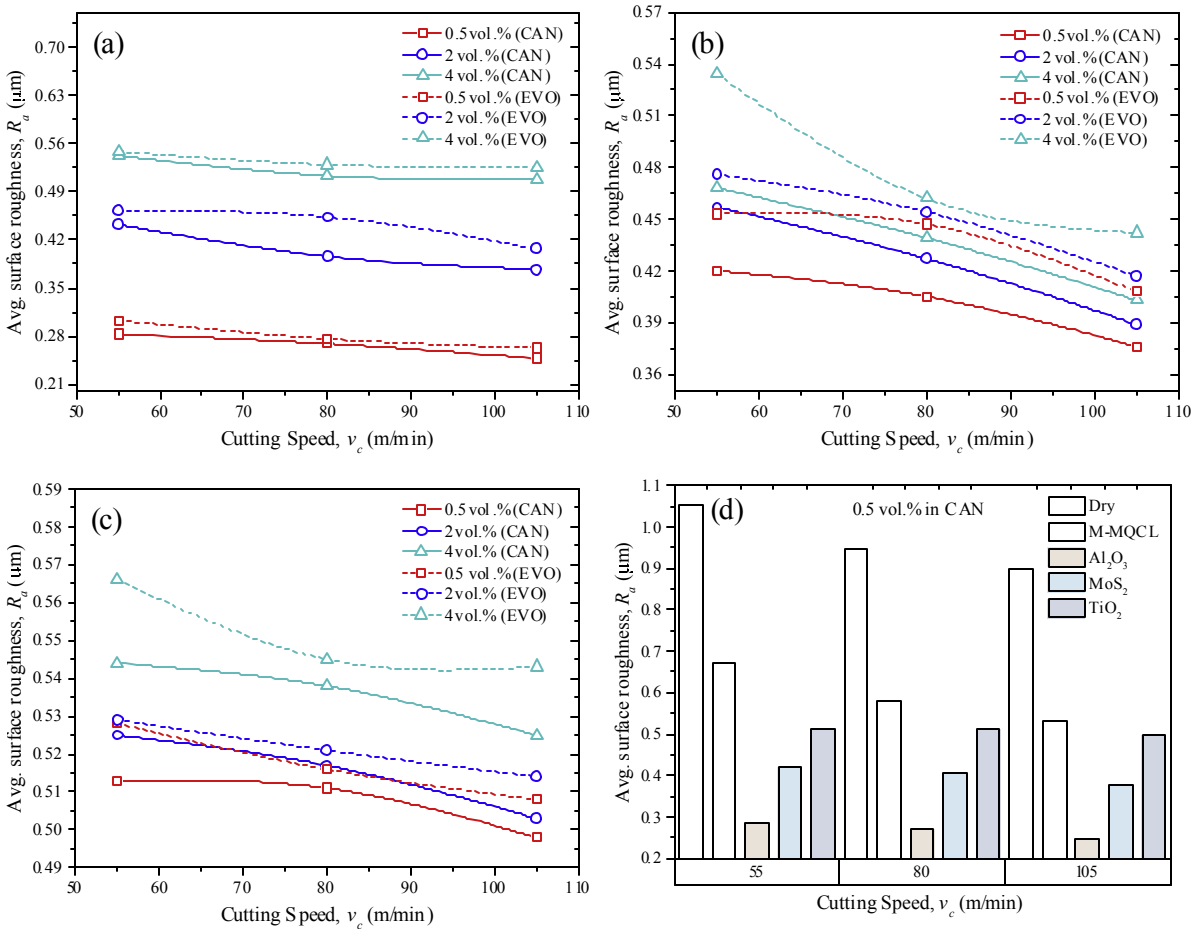


**Fig. 7.** The effects of $v_c$, vol% of (a) $Al_2O_3$, (b) $MoS_2$, and (c) $TiO_2$ nanoparticles, and types of VO on $R_a$; (d) the performance comparison of the nanofluids with M-MQCL and dry cutting.

Note that in eqn. (4), $s_o$ is representing the feed rate (0.1 mm/rev) and $\varphi$ is the shear angle (80°). It is known that $r_c$ is always less than 1, as the thickness of the chips increase after cut owing to almost all sided compression and friction at the chip-tool interface. The smaller value of $r_c$ is an indication of higher degree of compression stress, consequently, higher cutting forces and COF at contact interfaces. It is obvious from the upward trend of each of the curves that $r_c$ is greatly influenced by $v_c$, and $r_c$ gradually increased with the increase of $v_c$ (Fig. 12). That is likely attributed to the progressive changes in the tool geometry and the increase in cutting temperature due to tool wear (Dargusch et al., 2017). Moreover, cutting forces required to cut the material plummeted at high $v_c$, which led to reduced compression and friction at the chip-tool interface zone, as a result, low $t_c$ was recorded at high cutting speed, and therefore, smaller $r_c$. Furthermore, increment of $r_c$ with the decrease in vol%, as can be seen from the figure, is attributed to the reduction of COF. In contrast, interestingly, 2 vol% $Al_2O_3$-EVO provided much higher value of $r_c$ than 0.5 and 4 vol% (Fig. 12a). Here an analogous pattern like previous section (3.3) was observed, that is CAN rendered improved nanolubrication with $MoS_2$ and $TiO_2$ nanoparticles, while EVO with $Al_2O_3$ nanoparticles. It could be noticed that the highest $r_c$ value (0.92383 at $v_c$ of 105 m/min) was recorded for 0.5 vol% $MoS_2$-CAN, which set forth an increase of 38.1% as compared to dry cutting (at $v_c = 105$ m/min), while M-MQCL only raised the ratio by 9.6% (Fig. 12d). Noteworthy, at medium speed 0.5 vol% $TiO_2$ nanofluid accounted for 40.78% increase, while 0.5 vol% $MoS_2$-CAN augmented $r_c$ value by 36.4%. Nevertheless, at low cutting speed (55 m/min), 54.38% increase was observed for 0.5 vol% $MoS_2$-CAN.

Thermal conductivity of cutting insert plays a prominent role in absorbing and transferring heat away from contact surfaces. When chip-tool interface temperature is very high and thermal conductivity of cutting insert is sufficiently low, thermal gradient exists between chip sliding surface (back surface) and free surface. If the sliding surface temperature is higher than the free surface temperature the chip starts to curl to a smaller radius due to the existence of residual thermal stresses, and the chip behaves as a bi-metallic spring (Jawahir and Van Luttervelt, 1993). In this study, it was observed that dry cutting resulted in high chip curling frequency and compact chip curl radius (Fig. 13). However, the nanofluids facilitated the formation of semi-continuous chips with less curling through the reduction of thermal gradient.

SEM images of the chips (side view and back surface view) developed at dry cutting mode and 0.5 vol% $MoS_2$-CAN assisted MQCL condition are shown in Figs. 14 and Fig. 15, respectively. Overall, spiral and semi-continuous serrated chips (also known as saw-tooth or segmented chips) were observed in both conditions at the low cutting speed, which are considered to be caused by adiabatic shearing and thermoplastic instability – thermal softening predominates over strain hardening – due to the low thermal conductivity of the titanium alloy (Komanduri and Von Turkovich, 1981). For dry cutting (at 55 m/min of $v_c$), severe friction tracks and lateral flow of chip-material are obvious from the figure. Nevertheless, at 105 m/min of $v_c$, there is an apparent decrease in

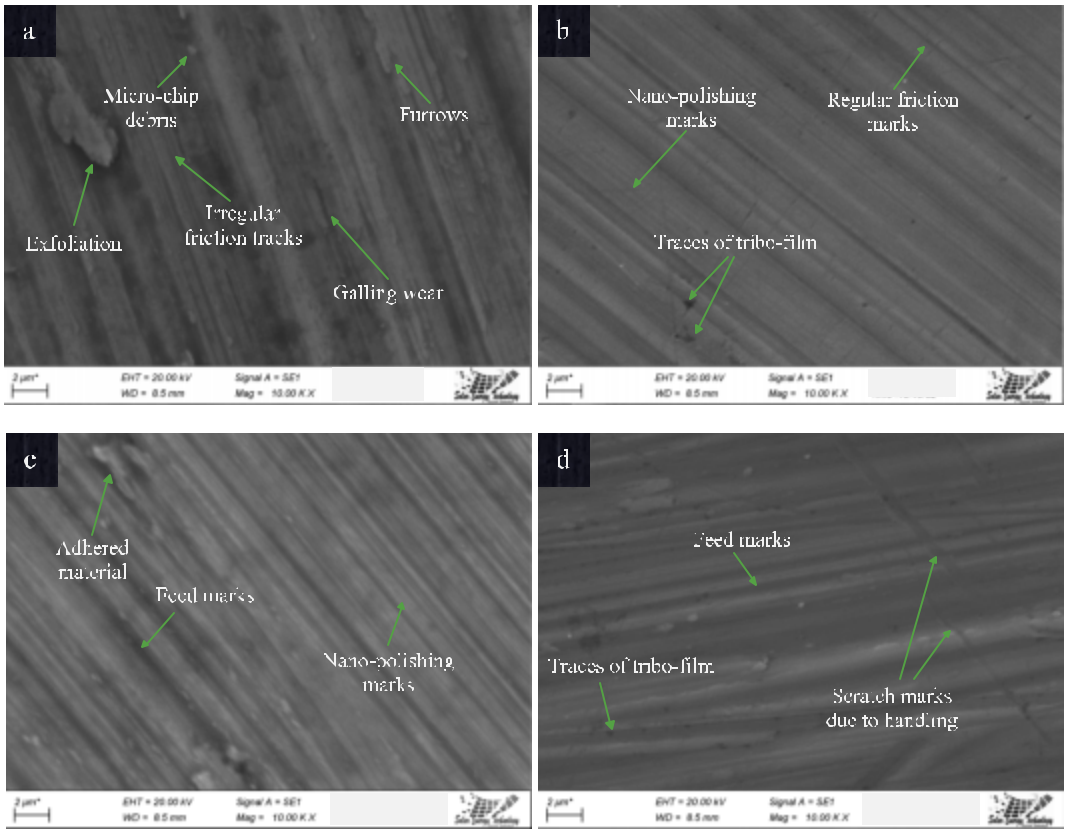


**Fig. 8.** SEM micrographs of the machined surfaces at (a) dry cutting mode, (b) 0.5 vol% $Al_2O_3$-CAN, (c) 0.5 vol% $MoS_2$-CAN, and (d) 0.5 vol% $TiO_2$-CAN nanofluid conditions.

friction tracks at the back surface of the chip that leads to the conclusion that there has been a reduction in friction force with the increase in $v_c$. The burr edges and irregular deformities are also frequent in the chip collected at 105 m/min. Furthermore, at the high cutting speed, thickness of the chip is found to be less, which is in accordance with the discussion stated in the previous paragraph. Although friction tracks are barely visible for 0.5 vol% $MoS_2$-CAN at 55 m/min, no traces of such marks are identified at 105 m/min. It is also seen that the nanofluid produced finer saw-tooth, as evidenced by the side view micrographs of the chips. This is an indication of stable cutting condition with minimum tool force fluctuation, which eventually manifests smooth ridges and valleys and yields low $R_a$ (Chan et al., 2013).

### 3.5. Tool wear

It is well documented that dissolution-diffusion is a dominant wear mechanism of WC tools during medium and high speed turning of titanium and its alloys. The high chip-tool interface temperature (~1000 °C), large cutting forces, low thermal conductivity, and strong chemical reactivity of titanium alloys promote diffusion of tool materials into chips, and foment adhesion of chip material to insert's rake face, which usually gets torn away by sliding chips leading to attrition wear. To investigate the wear mechanism and improvements offered by the nanofluid assisted MQCL, flank face and rake face of the cutting inserts for dry cutting mode and three different nanofluid assisted MQCL conditions were carefully examined. In essence, the cutting condition had pronounced implications on tool life, and lubrication and cooling using nanofluids resulted in lesser tool wear than that achieved at the dry cutting mode. It can be seen that, dry cutting leads to significant loss of tool material at the principal cutting edge and on the rake face, causing the recession of cutting edge and depth of crater wear. For all the nanofluids investigated in this section, there is a clear evidence of gradual wear (i.e., abrasion wear), revealing that nanofluid was not able to truncate COF sufficiently to prevent such wear; nevertheless, the application of nanofluid delayed the attrition wear, indicating increased tool life, as can be seen in Fig. 16. To assess the influence of the nanofluids over built-up edge formation (BUE), the rake faces of the cutting inserts were also analyzed and compared with the cutting insert collected after dry cutting (Fig. 17). BUE accelerates both crater wear and flank wear by flaking and chipping (Kamruzzaman et al., 2017), thus, eradication of it is essential. According to this analysis, the rake face of the cutting insert (Fig. 17d), used in the dry cutting mode, reveals the formation of BUE, while the nanofluids impeded the phenomenon. Noteworthy, BUE usually forms at low cutting speed, however, in this study at high cutting speed, BUE formation was detected for dry cutting, this is because of deposition of gummy titanium alloy to tool material at very high temperature. Monotonous improvement in terms of crater wear was also detected while using nanofluids and, rubbing and chipping were present in the rake face for all the cutting conditions.

## 4. Discussion

The amelioration of surface quality can be attributed to the mending effect (Liu et al., 2004) and the nano-polishing effect (Wang et al., 2017), while the reduction of chip-tool interface temperature in nanofluid aided cutting can be ascribed to the curtailment of COF mainly owing to the rolling mechanism (Tao et al., 1996), where nanoparticles act as nano-ball bearings, and

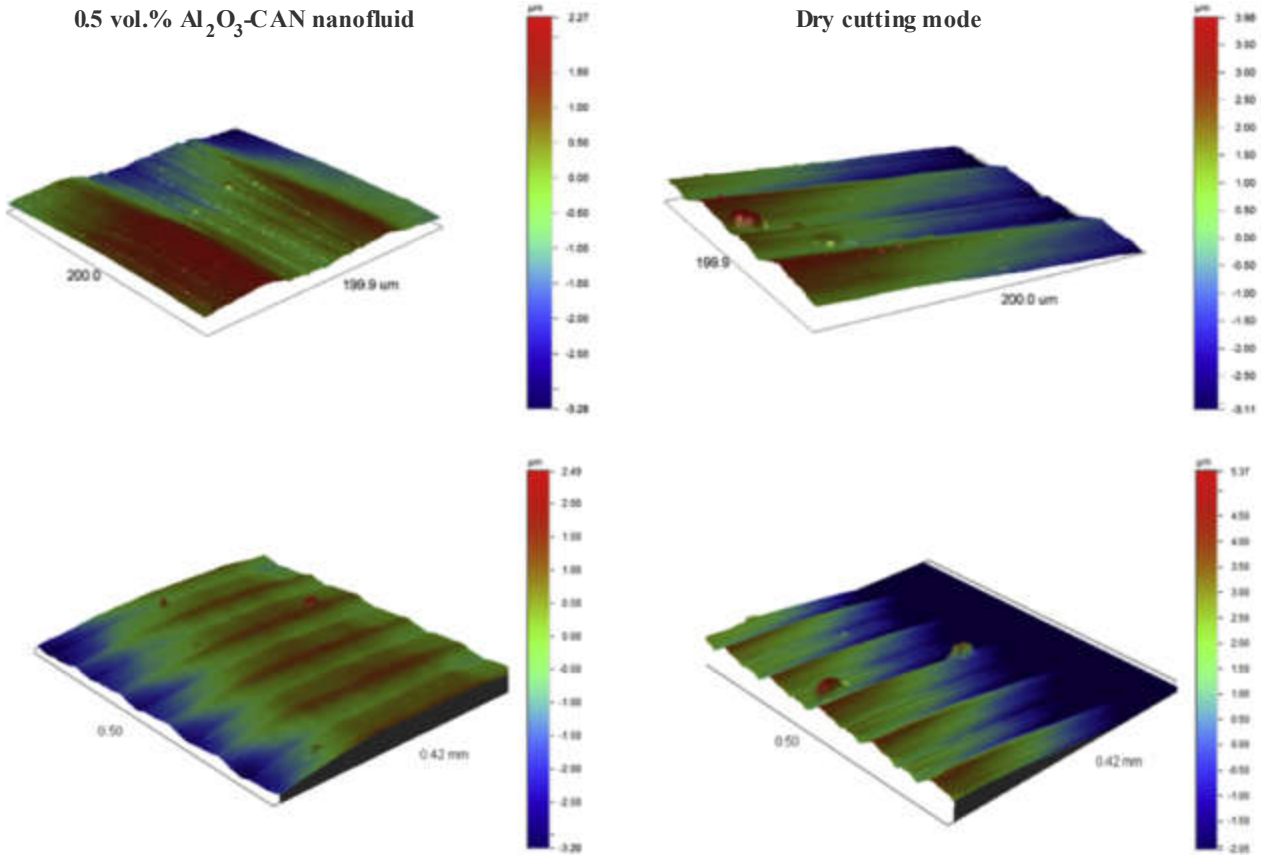


**Fig. 9.** 3D surface plots of the samples machined under 0.5 vol% $Al_2O_3$-CAN nanofluid-assisted MQCL condition and at dry cutting mode.

the formation of tribo-film (Wu et al., 2017) at tool and chip-workpiece interfaces. Other minor aspects of nanofluids that affect the heat dissipation from primary, secondary, and tertiary deformation zones in a subtle way are the increase in thermal conductivity, the reduction of specific heat capacity and contact angle.

Physical and chemical properties of the nanopartides are found to possess substantial influence over the tribological performance. $MoS_2$, for example, has shown better heat dissipation and scaling down of COF as compared to other nanoparticles due to its unique two-dimensional layered structure, where each 2D layer has a plane of hexagonally arranged Mo atoms sandwiched between two planes of hexagonally arranged S atoms, with covalently bonded S–Mo–S atoms in a trigonal prismatic arrangement forming a hexagonal crystal structure. These layers are held together by weak van der Waals forces. The van der Waals interactions between the neighboring layers are small compared to the strength of the Mo–S bond within the layer, and therefore, the layers can move with relative ease against each other. The sliding movement of the layers makes it an excellent lubricant additive. Furthermore, spherical $MoS_2$ nanoparticles play a very important role in reducing the COF, as particles undergo rotation and deformation followed by exfoliation of 2D-$MoS_2$ nanolayers during the wear process due to shear stress induced by the sliding surfaces. Exfoliated 2D-$MoS_2$ nanosheets adhere to the rubbing surfaces and eventually, form tribo-film (Dong et al., 2016), which acts as a third body and provides easy shear between the two metal surfaces. Each 2D crystal layer of $MoS_2$ is about 0.65 nm thick, while the thickness of the tribo-film is typically two to three monolayers (He and Que, 2016). In addition, due to high young modulus, spherical and quasi-spherical $MoS_2$ nanoparticles act as nano-ball bearings (rolling mechanism) –transfers sliding friction to a combination of sliding and rolling friction– before they gradually deform (Lahouij et al., 2012).

Likewise, $Al_2O_3$ and $TiO_2$ nanoparticles exhibit rolling mechanism between interacting surfaces; however, owing to very high hardness coupled with excellent anti-friction properties (Luo et al., 2014), the nano-polishing effect is the prevailing tribological property of $Al_2O_3$ nanoparticles (referring to Fig. 8). The attractiveness of nanoparticles also includes their ease of filling scars and grooves of the friction surface (mending effect), which is conducive for enhancing surface quality and minimizing asperity contact. $Al_2O_3$ and $TiO_2$ nanoparticles can also offer tribo-film formation effect (Ali et al., 2016); this tribo-film helps to protect the machined material from crack propagation by reducing friction between asperities (Gulzar et al., 2016).

Furthermore, heat conduction from contact surfaces to the MQCL droplets fosters full or partial evaporation of the droplets and the partial evaporation results in the formation of an intermediate vapor blanket, which minimizes the liquid and solid contact and hurdles heat transfer (Behera et al., 2017). Although air-atomized spray sweeps away most of the partially evaporated droplet, the formation of vapor layer cannot be eradicated. Nanofluid droplets have better thermal conductivity and do not go through partial evaporation, as a result, nanofluid MQCL prevail over the formation of vapor blanket.

The chip-tool contact length can be distinguished into the following two regions: seizure, which restricts the penetration of conventional cutting fluids as in this region chip and tool material remain in intimate contact and there is no relative motion, and slip,

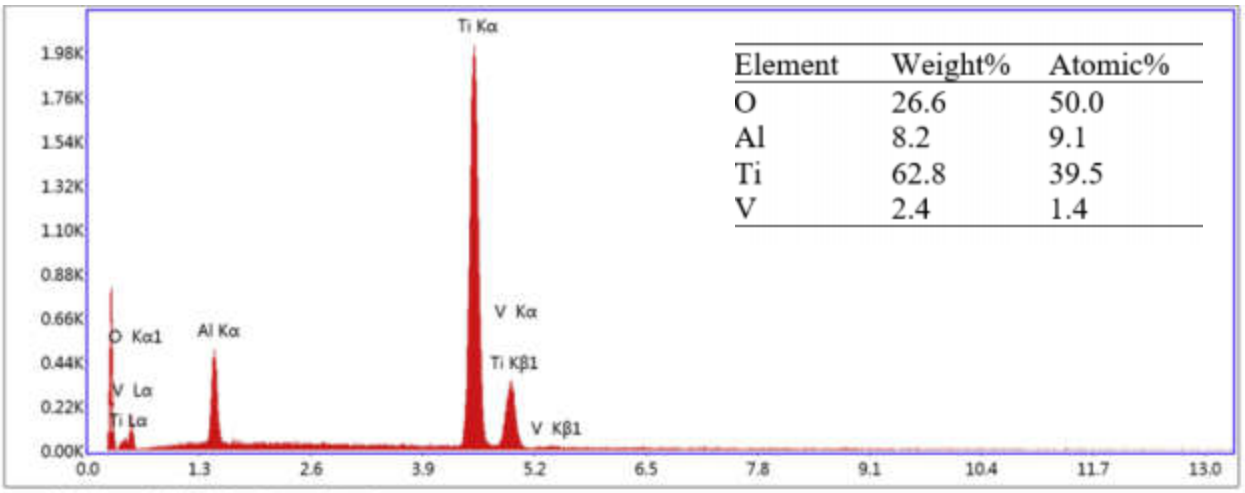


| Element | Weight% | Atomic% |
|---|---|---|
| O | 26.6 | 50.0 |
| Al | 8.2 | 9.1 |
| Ti | 62.8 | 39.5 |
| V | 2.4 | 1.4 |

a.

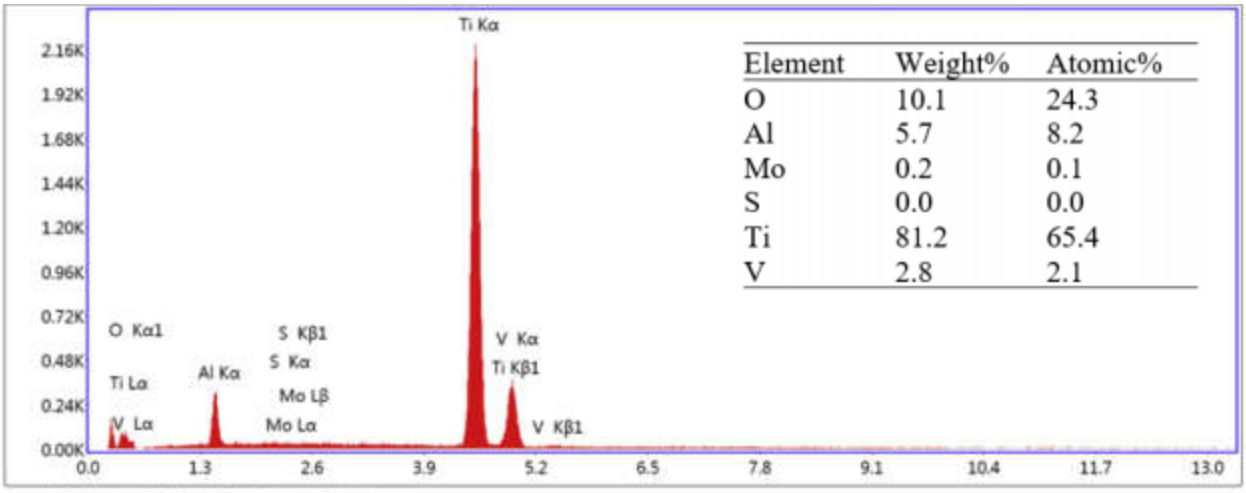


| Element | Weight% | Atomic% |
|---|---|---|
| O | 10.1 | 24.3 |
| Al | 5.7 | 8.2 |
| Mo | 0.2 | 0.1 |
| S | 0.0 | 0.0 |
| Ti | 81.2 | 65.4 |
| V | 2.8 | 2.1 |

b.

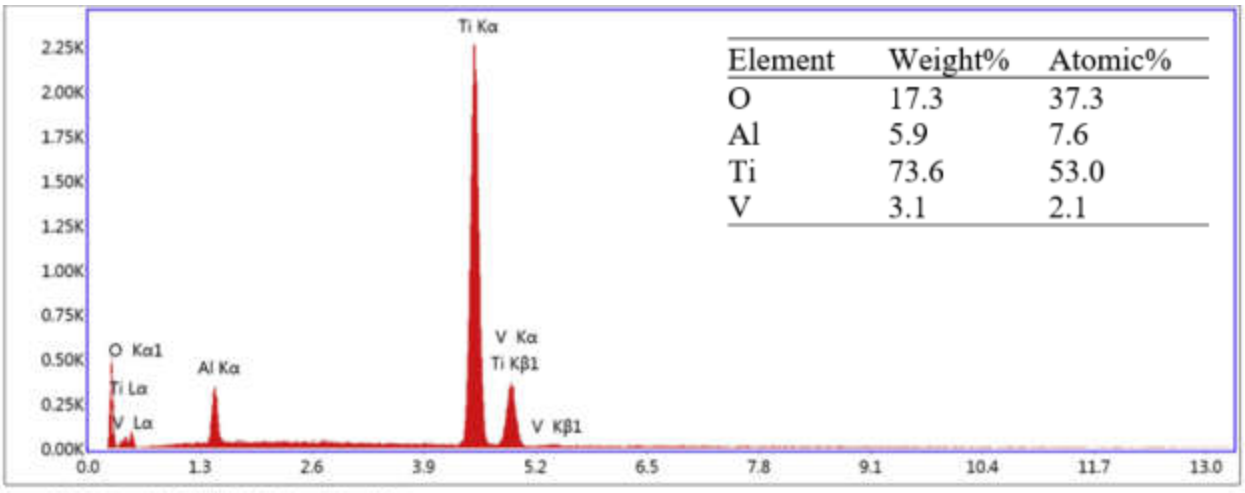


| Element | Weight% | Atomic% |
|---|---|---|
| O | 17.3 | 37.3 |
| Al | 5.9 | 7.6 |
| Ti | 73.6 | 53.0 |
| V | 3.1 | 2.1 |

c.

**Fig. 10.** EDS patterns and elemental contents of the surfaces machined using 0.5 vol% (a) $Al_2O_3$, (b) $MoS_2$, and (c) $TiO_2$-CAN nanofluids.

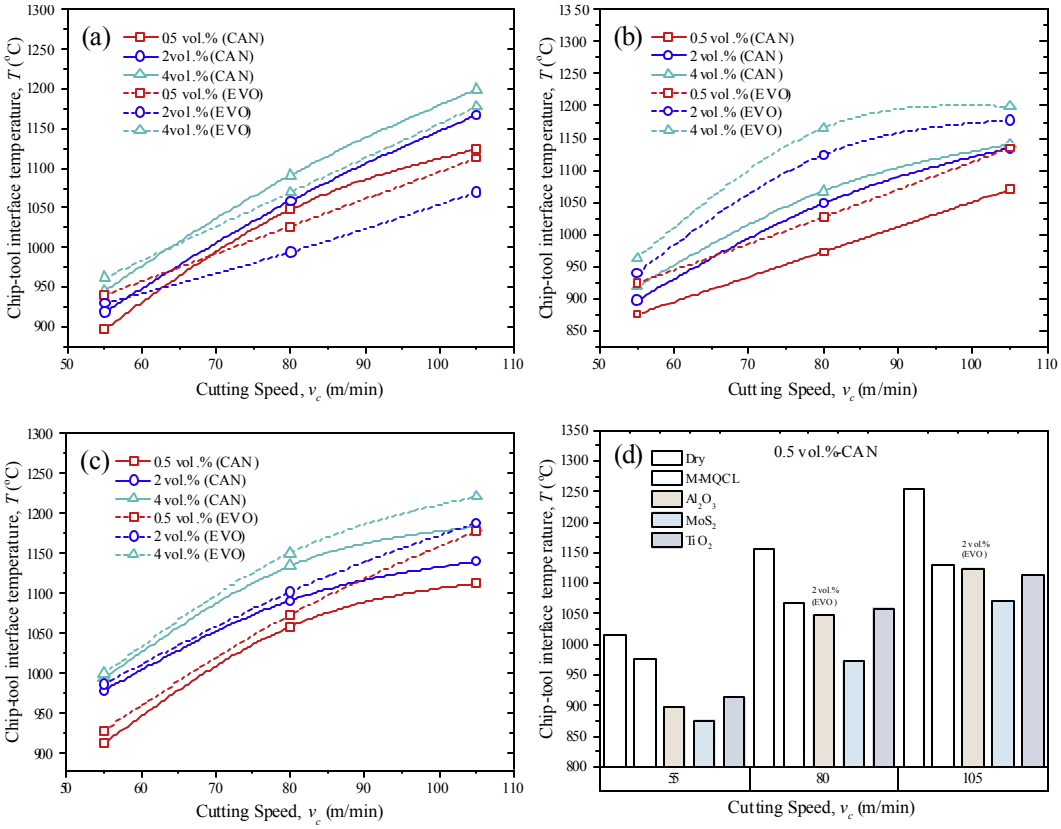


**Fig. 11.** The effects of $v_c$, vol% of (a) $Al_2O_3$, (b) $MoS_2$, and (c) $TiO_2$ nanoparticles, and types of VO on $T$; (d) the performance comparison of the nanofluids with M-MQCL and dry cutting.

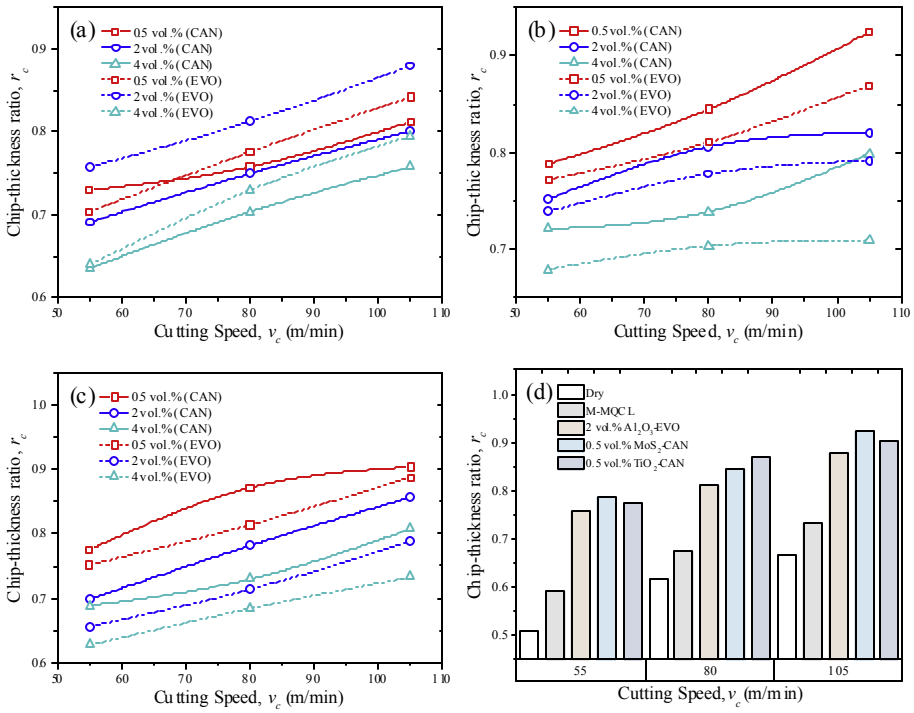


**Fig. 12.** The effects of $v_c$, vol% of (a) $Al_2O_3$, (b) $MoS_2$, and (c) $TiO_2$ nanoparticles, and types of VO on $r_c$; (d) the performance comparison of the nanofluids with M-MQCL and dry cutting.

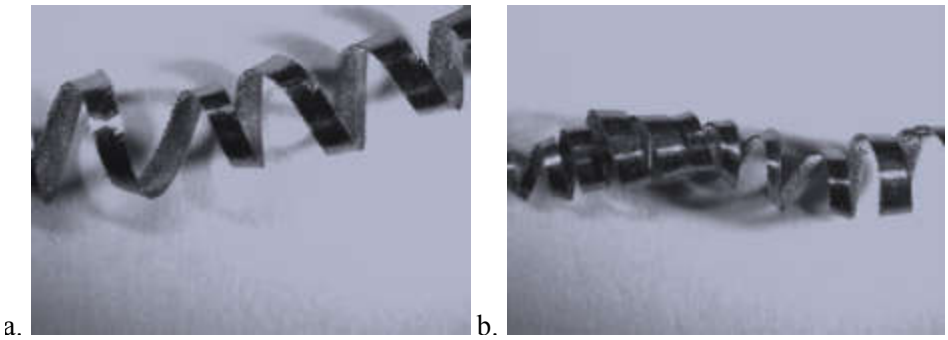


**Fig. 13.** Chips formed at (a) 0.5 vol% $MoS_2$-CAN assisted MQCL and (b) dry cutting mode.

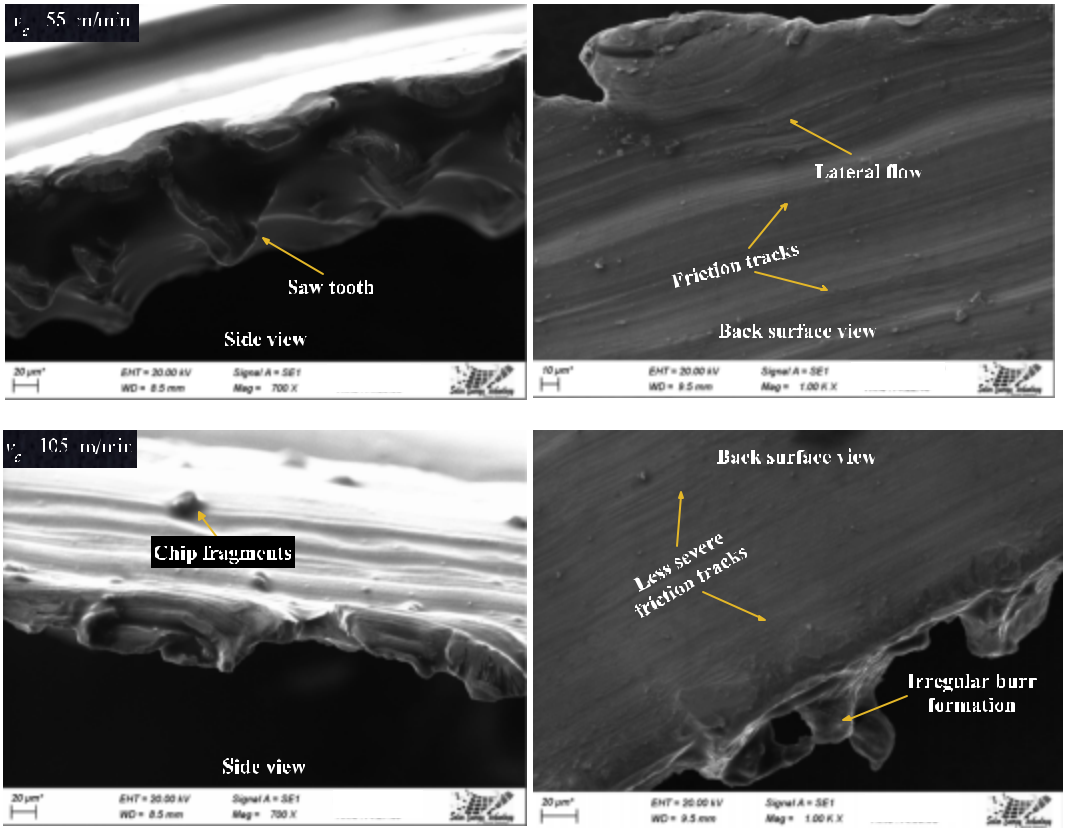


**Fig. 14.** SEM images of side surface and back surface of chips generated at dry cutting.

where coolant can reach and lubricate effortlessly (Trent, 1988). A plausible rationale for wear eradication (specially attrition wear) under nanofluid application is that nanoparticles, due to their size, are able to penetrate through the seizure region and truncate the area of seizure to some extent, therefore, COF and cutting temperature declines substantially, which is vital to impede severe tool wear.

The effect possessed by nanoparticle concentration was more conspicuous than any other factors considered in this article. In general, 0.5 vol% provided superior results in terms of $R_a$, $T$, and $r_c$. Referring to section 3, it was observed that the kinematic and dynamic viscosity of the nanofluids increased with the increase in vol %. The heat transfer coefficient of nanofluids has a negative correlation with viscosity, thus less concentrated nanofluids was found to be more effective in heat dissipation. Moreover, lower value of viscosity aids to minimize viscous force thereby, reduces asperity friction between sliding surfaces, which is essential for the reduction of frictional power losses. A well-organized description of the role of nanoparticle concentration on viscosity of nanofluids was published by Li et al. (2017).

In a compelling demonstration of the influence of contact angle on the cooling efficiency of grinding cutting fluid, Zhang et al. (2016) stated an explanation from heat convection point of view, which can also be used to describe why small contact angle of the droplets provides higher cooling competency in turning operations. The profile of a droplet can be divided into thermal boundary layer (viscous layer and turbulence layer) and main flow region during heat convection. The main flow region is basically carried away from cutting zone by sliding movement of cutting insert and deformed chips (at chip-tool interface), while thickness of the thermal boundary layer remains almost entirely equivalent and stable. The thermal boundary layer widens as the contact angle of a

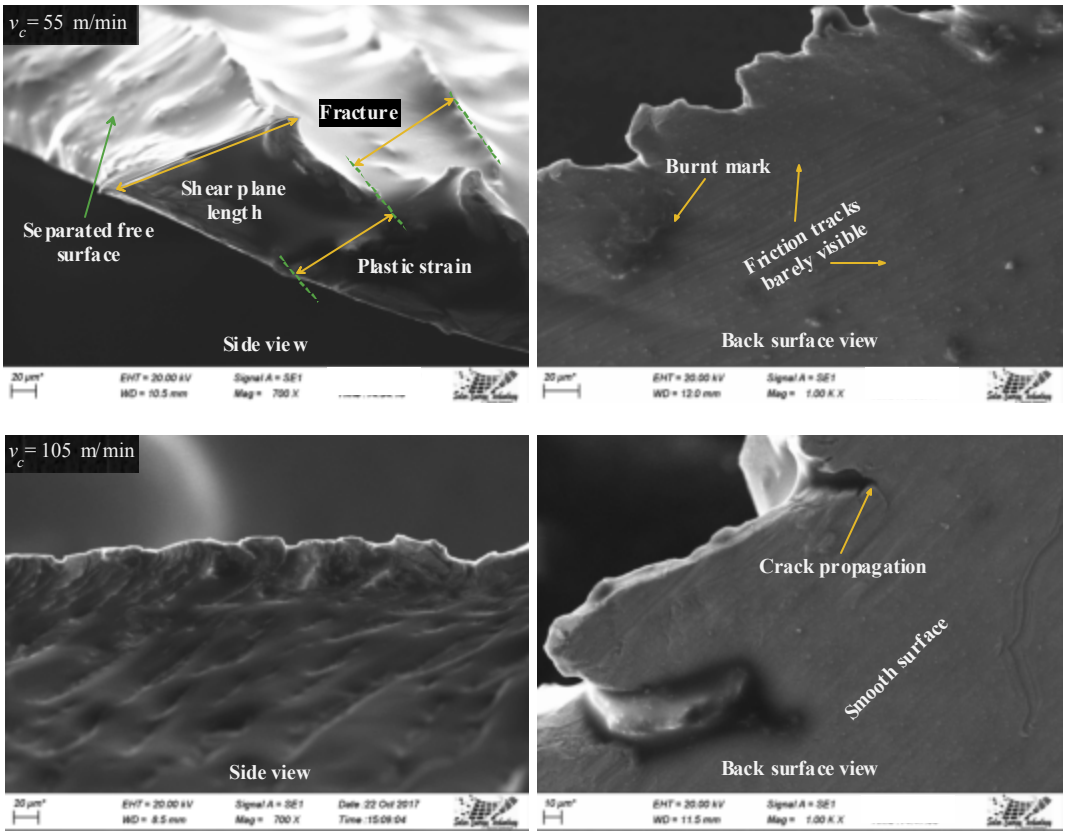


**Fig. 15.** SEM images of side surface and back surface of chips generated at 0.5 vol% $MoS_2$-CAN nanofluid assisted MQCL.

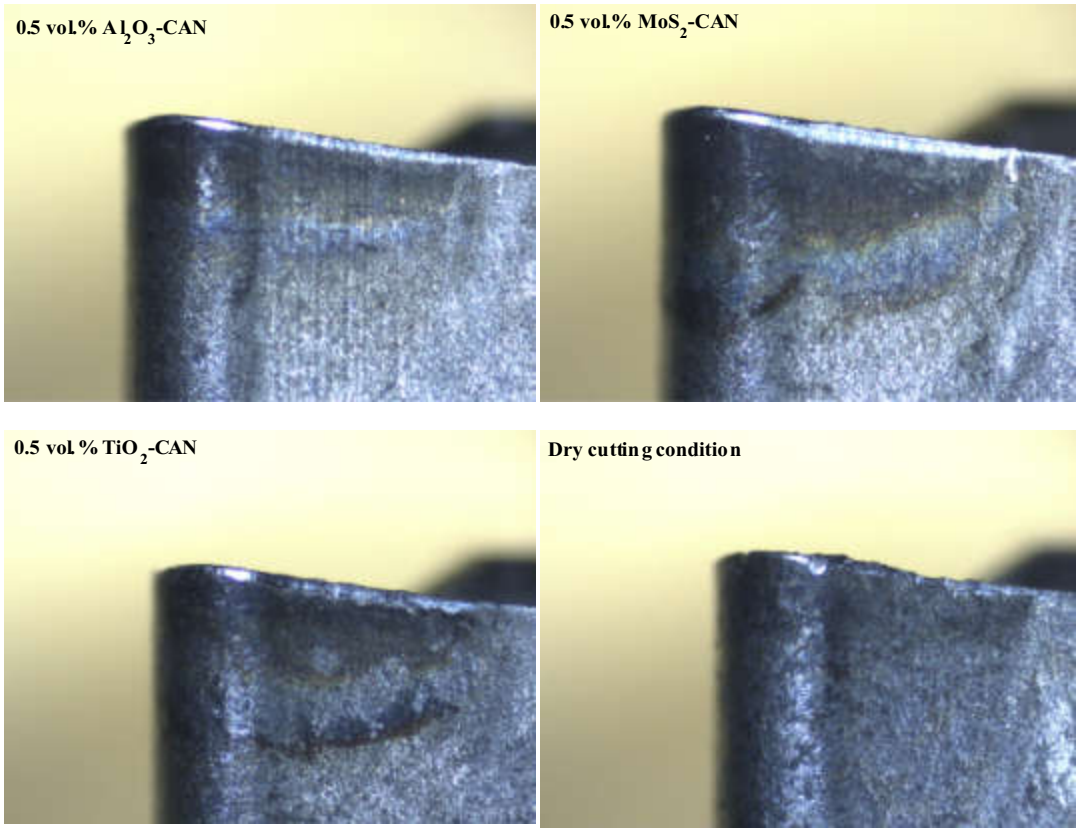


**Fig. 16.** Flank wear of the cutting inserts at different cutting conditions.

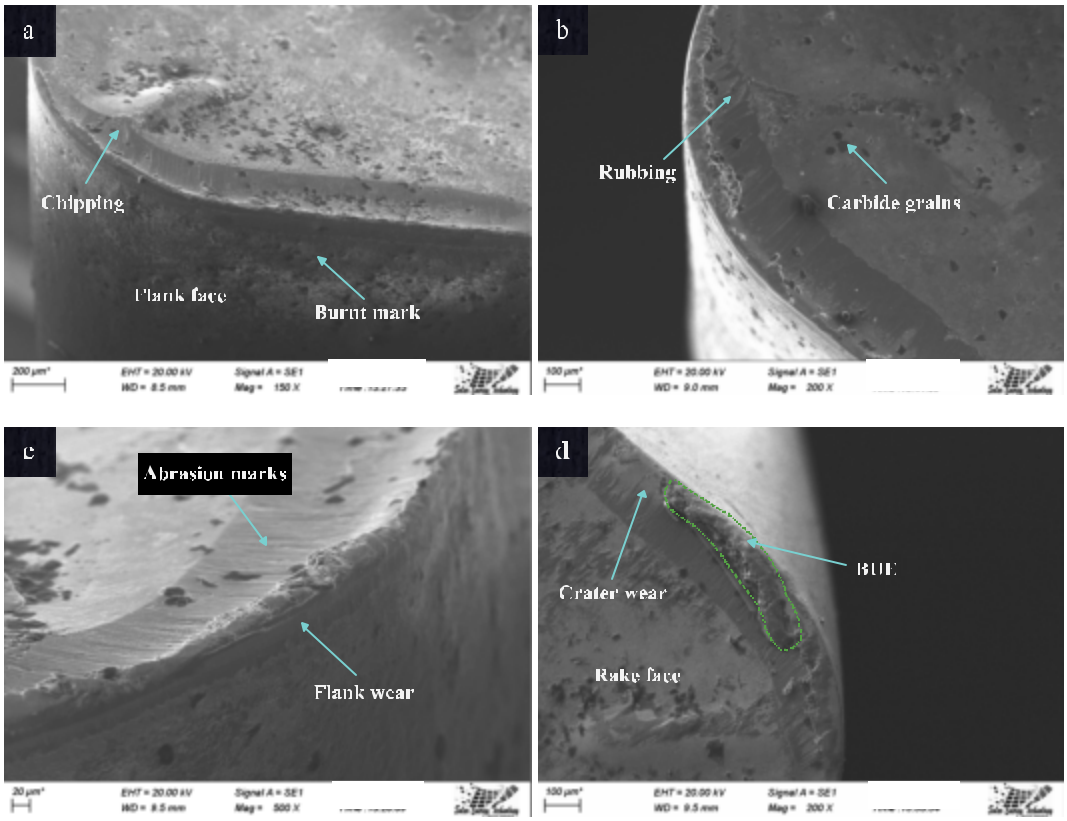


**Fig. 17.** Rake face of the cutting inserts used in 0.5 vol% (a) $Al_2O_3$-CAN, (b) $MoS_2$-CAN, and (c) $TiO_2$-CAN nanofluid assisted MQCL turning and (d) dry cutting mode.

droplet decreases thus, overall proportion of liquid present in the main flow region declines. This enables better heat extraction from the cutting zone and the chip-tool interface. Moreover, small droplet contact angle results in much more effective delivery of nanofluids in between contact surfaces (Cha et al., 2013). The term wettability describes the contact between a liquid and a solid surface. The amount of wetting depends on the energies of the interfaces involved. A contact angle of $\theta = 0°$ represents a perfectly wetting condition and $\theta = 180°$ represents a perfectly non-wetting condition. The maximum wetting area per unit liquid volume expands as contact angle decreases (Wang et al., 2017). This, eventually, leads to improved tribological performance at the contact interfaces. If the concentration exceeds the threshold limit then nanoparticles tend to form micro-clusters and agglomeration rate rapidly increases, as a result, nanofluids loses its' effectiveness considerably. For $Al_2O_3$-EVO nanofluid, 2 vol% is found to be the optimum concentration while agglomeration of nanoparticles started to occur at 4 vol%. On the other hand, 1 vol% of $Al_2O_3$ was not sufficient enough to provide outstanding results as evidenced by the results obtained in $T$ and $r_c$ experiments. To understand this phenomenon, an independent molecular dynamic study is needed, which is not the scope of this article. Nevertheless, our findings are in accordance with the study conducted by Rahmati et al. (2014), where authors claimed that 0.5 wt% $MoS_2$ provided better surface finish compared to 0.2 and 1 wt%. Similarly, Rapeti et al. (2018) showed that 0.5% $MoS_2$ inclusion in coconut oil leads to minimum cutting force, cutting temperature, tool wear, and surface roughness.

CAN, paradoxically, provided better lubrication and cooling performance than EVO, although, the later one has relatively higher thermal conductivity and lower kinematic viscosity. Perhaps, thermal conductivity and viscosity of vegetable oils may not necessarily play a deterministic role, since the performance is shown not to be dictated by these properties. Instead, the molecular structure, carbon chains, other constituents of vegetable oils may become important due to associated chemical reaction with metal surface induced at very high temperature during machining. CAN and EVO primarily consist of triacylglycerides, which have glycerol molecules with three long fatty acid chain attached at the hydroxyl groups via ester linkages (Fox and Stachowiak, 2007). The long and polar fatty acid chains provide favorable characteristics for boundary lubrication, for example, adsorption, which refers to the adhesion of polar heads of triglycerides to the metal surface, and tribo-film, which forms as a result of the replacement of the hydrogen atoms in carboxyl −COOH by atoms from the metal surface. Oleic acid (18 carbons), the main fatty acid type in CAN and EVO, is monounsaturated omega-9 fatty acid. As can be seen from Table 5 that oleic acid content of EVO (71%) is higher than CAN (62%). Adhvaryu et al. (2006) claimed that oleic acid content has inverse effect on the free energy of adsorption, consequently, on overall lubrication, as they observed lower COF for canola (0.092) than olive oil (0.112). This explanation fits well for the single-phase model of nanofluids; however, the state becomes convoluted for two-phase model, as the physicochemical reactions between nanoparticles, fatty acids, and fluid molecules also have to be considered. The outcome of these reactions irrefutably plays a vital role in the effectiveness of nanolubrication and determining the strength of tribo-film, which necessitates further nanotribological studies to comprehend the phenomenon. This is of course a very challenging task, which is completely beyond the scope of the present work.

VOs are increasingly used as a substitute for fossil fuel based industrial lubricants owing to their high biodegradability, non-toxicity, low production cost and environmental pollution, and

high fire and flash point (Shashidhara and Jayaram, 2010). An overwhelming amount of scientific data supports using VOs as potential cutting fluids. While conventional cutting fluids cause allergic and irritant contact dermatitis and respiratory diseases (Debnath et al., 2014), VOs, on the other hand, possesses no occupational health risks. Pereira et al. (2016) presented a detailed study from ecological point of view and concluded that MQCL technique (0.178 kg−$CO_2$−eq) is eco-friendlier than conventional wet machining (0.193 kg−$CO_2$−eq) and even dry machining (0.202 kg−$CO_2$−eq) in terms of global warming. Although, toxicity of nanoparticles and nanomaterials are still disputable in the scientific community, toxicity levels of VO based nanofluids is substantially less than fossil fuel based cutting fluids; moreover, the use of MQCL further subjugates negative impacts of nanoparticles on health and environment, and restricts accumulation of nanoparticles into the aquatic, terrestrial, and atmospheric environment as well as minimizes the increasing risk of creating nano-waste, which is considered as a new potential threat to the environment.

## 5. Conclusions

In summary, the observations that are presented here indicate that the two engineered nanofluids coupled with MQCL have the necessary attributes to be considered as attractive alternatives for toxic and environmentally harmful metal cutting lubricants, and expensive lubrication and cooling delivery technologies. Herein, the lowest $R_a$ value (0.248 μm) was recorded for 0.5 vol% $Al_2O_3$-CAN nanofluid, which is strikingly 73.1% and 57.95% less than that recorded for dry cutting and M-MQCL modes at 55 m/min of $v_c$. However, on the other hand, 0.5 vol% $MoS_2$ outperformed other nanofluids in terms cooling, as the lowest $T$ (875 °C) and the highest $r_c$ (0.9238) were recorded for the application of this fine-tuned nanofluid, which are rudimentary indications of substantial decrease in cutting forces and COF. Further, nanofluid aided MQCL delayed the attrition wear and controlled the flank wear expedition of cutting insert. The present results also reveal that the increase in nanoparticle concentration led to the decrease of nanolubrication effectiveness, and CAN is a better option than EVO as base fluid. Recapitulation of SEM analysis is that 0.5 vol% $Al_2O_3$-CAN nanofluid inhibited surface defects and imparted highly smooth surface texture. In addition to that, although scuffing wear was readily identifiable in the dry cut surface, nanolubrication enhanced scuffing resistance of the titanium alloy, which will ensure longer component lifetime. In essence, understanding the factors that influence the nanolubrication performance in turning operation provide insights for improving the existing nanofluids and designing new nanofluids with superior tribological properties for metal cutting of super alloys. This study opens up several new avenues for fundamental studies and potential applications.

## Funding

This research did not receive any specific grant from funding agencies in the public, commercial, or not-for-profit sectors.

## Acknowledgement

The authors would like to thank the respected reviewers, Prof. Dr. Ahmed Sharif, Md. Kabir Hossain, Khandaker Shamail Hossain, Prof. Dr. Dewan Hasan Ahmed, and Munira Sultana for their experimental assistance and/or inspiring discussion. This research used resources of the Institute of Fuel Research and Development (IFRD), Bangladesh Council of Scientific and Industrial Research (BCSIR). Royal CNC Training Institute is acknowledged for providing necessary support.

## References

Abdalla, H., Baines, W., McIntyre, G., Slade, C., 2007. Development of novel sustainable neat-oil metal working fluids for stainless steel and titanium alloy machining. Part 1. Formulation development. Int. J. Adv. Manuf. Technol. 34, 21–33.
Adhvaryu, A., Biresaw, G., Sharma, B.K., Erhan, S.Z., 2006. Friction behavior of some seed oils: biobased lubricant applications. Ind. Eng. Chem. Res. 45, 3735–3740.
Ali, M.A.M., Azmi, A.I., Khalil, A.N.M., Leong, K.W., 2017. Experimental study on minimal nanolubrication with surfactant in the turning of titanium alloys. Int. J. Adv. Manuf. Technol. 1–11.
Ali, M.K.A., Xianjun, H., Mai, L., Qingping, C., Turkson, R.F., Bicheng, C., 2016. Improving the tribological characteristics of piston ring assembly in automotive engines using $Al_2O_3$ and $TiO_2$ nanomaterials as nano-lubricant additives. Tribol. Int. 103, 540–554.
Altintas, Y., 2012. Manufacturing Automation: Metal Cutting Mechanics, Machine Tool Vibrations, and CNC Design. Cambridge university press.
Behera, B., Ghosh, S., Rao, P., 2016. Application of nanofluids during minimum quantity lubrication: a case study in turning process. Tribol. Int. 101, 234–246.
Behera, B.C., Setti, D., Ghosh, S., Rao, P.V., 2017. Spreadability studies of metal working fluids on tool surface and its impact on minimum amount cooling and lubrication turning. J. Mater. Process. Technol. 244, 1–16.
Chan, C., Lee, W., Wang, H., 2013. Enhancement of surface finish using water-miscible nano-cutting fluid in ultra-precision turning. Int. J. Mach. Tool Manufact. 73, 62–70.
Chieruzzi, M., Cerritelli, G.F., Miliozzi, A., Kenny, J.M., 2013. Effect of nanoparticles on heat capacity of nanofluids based on molten salts as PCM for thermal energy storage. Nanoscale research letters 8 (1), 448.
Dargusch, M.S., Sun, S., Kim, J.W., Li, T., Trimby, P., Cairney, J., 2017. Effect of tool wear evolution on chip formation during dry machining of Ti-6Al-4V alloy. Int. J. Mach. Tool Manufact.
Debnath, S., Reddy, M.M., Yi, Q.S., 2014. Environmental friendly cutting fluids and cooling techniques in machining: a review. J. Clean. Prod. 83, 33–47.
Dhar, N., Kamruzzaman, M., Ahmed, M., 2006. Effect of minimum quantity lubrication (MQL) on tool wear and surface roughness in turning AISI-4340 steel. J. Mater. Process. Technol. 172, 299–304.
Dong, C., Yuan, C., Wang, L., Liu, W., Bai, X., Yan, X., 2016. Tribological properties of water-lubricated rubber materials after modification by $MoS_2$ nanoparticles. Sci. Rep. 6.
Ezugwu, E., Wang, Z., 1997. Titanium alloys and their machinability—a review. J. Mater. Process. Technol. 68, 262–274.
Fox, N., Stachowiak, G., 2007. Vegetable oil-based lubricants—a review of oxidation. Tribol. Int. 40, 1035–1046.
Gulzar, M., Masjuki, H., Kalam, M., Varman, M., Zulkifli, N., Mufti, R., Zahid, R., 2016. Tribological performance of nanoparticles as lubricating oil additives. J. Nanoparticle Res. 18, 223.
He, Z., Que, W., 2016. Molybdenum disulfide nanomaterials: structures, properties, synthesis and recent progress on hydrogen evolution reaction. Applied Materials Today 3, 23–56.
Hegab, H., Umer, U., Deiab, I., Kishawy, H., 2018. Performance evaluation of Ti–6Al–4V machining using nano-cutting fluids under minimum quantity lubrication. Int. J. Adv. Manuf. Technol. 1–13.
Hoyne, A.C., Nath, C., Kapoor, S.G., 2015. On cutting temperature measurement during titanium machining with an atomization-based cutting fluid spray system. J. Manuf. Sci. Eng. 137, 024502.
Jawahir, I., Van Luttervelt, C., 1993. Recent developments in chip control research and applications. CIRP Ann. - Manuf. Technol. 42, 659–693.
Jin, C., Tang, Y., Yang, F.G., Li, X.L., Xu, S., Fan, X.Y., Huang, Y.Y., Yang, Y.J., 2011. Cellular toxicity of TiO2 nanoparticles in anatase and rutile crystal phase. Biol. Trace Elem. Res. 141, 3–15.
Kamruzzaman, M., Rahman, S.S., Ashraf, M.Z.I., Dhar, N.R., 2017. Modeling of chip–tool interface temperature using response surface methodology and artificial neural network in HPC-assisted turning and tool life investigation. Int. J. Adv. Manuf. Technol. 90, 1547–1568.
Kim, J., Kang, Y.T., Choi, C.K., 2004. Analysis of convective instability and heat transfer characteristics of nanofluids. Phys. Fluid. 16, 2395–2401.
Klocke, F., Eisenblätter, G., 1997. Dry cutting. CIRP Ann. - Manuf. Technol. 46, 519–526.
Komanduri, R., Von Turkovich, B., 1981. New observations on the mechanism of chip formation when machining titanium alloys. Wear 69, 179–188.
Lahouij, I., Dassenoy, F., Vacher, B., Martin, J.-M., 2012. Real time TEM imaging of compression and shear of single fullerene-like MoS2 nanoparticle. Tribol. Lett. 45, 131–141.
Lawal, S., Choudhury, I., Nukman, Y., 2012. Application of vegetable oil-based metalworking fluids in machining ferrous metals—a review. Int. J. Mach. Tool Manufact. 52, 1–12.
Leidenfrost, J.G., 1966. On the fixation of water in diverse fire. Int. J. Heat Mass Tran. 9, 1153–1166.
Li, B., Li, C., Zhang, Y., Wang, Y., Jia, D., Yang, M., Zhang, N., Wu, Q., Han, Z., Sun, K., 2017. Heat transfer performance of MQL grinding with different nanofluids for Ni-based alloys using vegetable oil. J. Clean. Prod. 154, 1–11.
Liu, G., Li, X., Qin, B., Xing, D., Guo, Y., Fan, R., 2004. Investigation of the mending effect and mechanism of copper nano-particles on a tribologically stressed surface. Tribol. Lett. 17, 961–966.

Luo, T., Wei, X., Huang, X., Huang, L., Yang, F., 2014. Tribological properties of $Al_2O_3$ nanoparticles as lubricating oil additives. Ceram. Int. 40, 7143–7149.
Padmini, R., Krishna, P.V., Rao, G.K.M., 2016. Effectiveness of vegetable oil based nanofluids as potential cutting fluids in turning AISI 1040 steel. Tribol. Int. 94, 490–501.
Pak, B.C., Cho, Y.I., 1998. Hydrodynamic and heat transfer study of dispersed fluids with submicron metallic oxide particles. Experimental Heat Transfer an International Journal 11, 151–170.
Pereira, O., Rodríguez, A., Fernández-Abia, A., Barreiro, J., de Lacalle, L.L., 2016. Cryogenic and minimum quantity lubrication for an eco-efficiency turning of AISI 304. J. Clean. Prod. 139, 440–449.
Rahman, S.S., Ashraf, M.Z.I., Bashar, M., Kamruzzaman, M., Amin, A.N., Hossain, M., 2017. Crystallinity, surface morphology, and chemical composition of the recast layer and rutile-$TiO_2$ formation on Ti-6Al-4V ELI by wire-EDM to enhance biocompatibility. Int. J. Adv. Manuf. Technol. 93, 3285–3296.
Rahmati, B., Sarhan, A.A., Sayuti, M., 2014. Morphology of surface generated by end milling AL6061-T6 using molybdenum disulfide ($MoS_2$) nanolubrication in end milling machining. J. Clean. Prod. 66, 685–691.
Rapeti, P., Pasam, V.K., Gurram, K.M.R., Revuru, R.S., 2018. Performance evaluation of vegetable oil based nano cutting fluids in machining using grey relational analysis-A step towards sustainable manufacturing. J. Clean. Prod. 172, 2862–2875.
Revuru, R.S., Posinasetti, N.R, VSN, V.R., Amrita, M., 2017. Application of cutting fluids in machining of titanium alloys—a review. Int. J. Adv. Manuf. Technol. 91, 2477–2498.
Sharma, A.K., Tiwari, A.K., Dixit, A.R., 2016a. Effects of Minimum Quantity Lubrication (MQL) in machining processes using conventional and nanofluid based cutting fluids: a comprehensive review. J. Clean. Prod. 127, 1–18.
Sharma, A.K., Tiwari, A.K., Singh, R.K., Dixit, A.R., 2016b. Tribological investigation of $TiO_2$ nanoparticle based cutting fluid in machining under minimum quantity lubrication (MQL). Mater. Today: Proceedings 3, 2155–2162.
Shashidhara, Y., Jayaram, S., 2010. Vegetable oils as a potential cutting fluid—an evolution. Tribol. Int. 43, 1073–1081.
Shahidzadeh, N., Schut, M.F., Desarnaud, J., Prat, M., Bonn, D., 2015. Salt stains from evaporating droplets. Sci. Rep. 5, 10335.
Sahoo, B.C., Vajjha, R.S., Ganguli, R., Chukwu, G.A., Das, D.K., 2009. Determination of rheological behavior of aluminum oxide nanofluid and development of new viscosity correlations. Petrol. Sci. Technol. 27 (15), 1757–1770.
Sidik, N.A.C., Samion, S., Ghaderian, J., Yazid, M.N.A.W.M., 2017. Recent progress on the application of nanofluids in minimum quantity lubrication machining: a review. Int. J. Heat Mass Tran. 108, 79–89.
Tannous, J., Dassenoy, F., Lahouij, I., Le Mogne, T., Vacher, B., Bruhács, A., Tremel, W., 2011. Understanding the tribochemical mechanisms of IF-$MoS_2$ nanoparticles under boundary lubrication. Tribol. Lett. 41, 55–64.
Tao, X., Jiazheng, Z., Kang, X., 1996. The ball-bearing effect of diamond nanoparticles as an oil additive. J. Phys. Appl. Phys. 29, 2932.
Trent, E.M., 1988. Metal cutting and the tribology of seizure: II movement of work material over the tool in metal cutting. Wear 128, 47–64.
Vasu, V., Pradeep Kumar Reddy, G., 2011. Effect of minimum quantity lubrication with $Al_2O_3$ nanoparticles on surface roughness, tool wear and temperature dissipation in machining Inconel 600 alloy. Proc. Inst. Mech. Eng. - Part N J. Nanoeng. Nanosyst. 225, 3–16.
Wang, Y., Li, C., Zhang, Y., Yang, M., Zhang, X., Zhang, N., Dai, J., 2017. Experimental evaluation on tribological performance of the wheel/workpiece interface in minimum quantity lubrication grinding with different concentrations of $Al_2O_3$ nanofluids. J. Clean. Prod. 142, 3571–3583.
Wu, H., Zhao, J., Xia, W., Cheng, X., He, A., Yun, J.H., Wang, L., Huang, H., Jiao, S., Huang, L., 2017. A study of the tribological behaviour of $TiO_2$ nano-additive water-based lubricants. Tribol. Int. 109, 398–408.
Yadav, D., Kumar, R., Naruka, D.S., Singh, P.K., 2017. Experimental Investigation on Viscosity of the Nanofluids with Different Parameters.
Zhang, Y., Li, C., Yang, M., Jia, D., Wang, Y., Li, B., Hou, Y., Zhang, N., Wu, Q., 2016. Experimental evaluation of cooling performance by friction coefficient and specific friction energy in nanofluid minimum quantity lubrication grinding with different types of vegetable oil. J. Clean. Prod. 139, 685–705.
Zhou, S.Q., Ni, R., 2008. Measurement of the specific heat capacity of water-based Al 2 O 3 nanofluid. Appl. Phys. Lett. 92 (9), 093123.